

# Layered Perovskite-Like Oxides 0112 Type: Structure, Properties, and Possible Applications

Andrei Klyndyuk

Belarus State Technological University, 220050 Minsk, Belarus

**Abstract.** Data available in the literature on layered  $LnAMe_2O_{5+\delta}$  ( $Ln$  – rare-earth element (REE); A – alkaline element (AE) or alkali-earth element (AEE); Me – 3d-metal) oxides related to the 0112 ( $YBaCuFeO_5$ ) structural type are summarized and discussed. The methods of preparation, crystal structure and thermal stability of the  $LnAMe_2O_{5+\delta}$  are described and their thermal expansion, magnetic and electrical properties are characterized. The influence of the REE and 3d-metal nature as well as the oxygen non-stoichiometry value on the structure and properties of these phases are analyzed. The influence of the oxygen sub-lattice state of  $LnAMe_2O_{5+\delta}$  phases on their properties as well as the phase transitions taking place in these oxides in a wide temperature range are discussed. It is shown that large values of electrical conductivity and thermo-e.m.f. values of some  $LnAMe_2O_{5+\delta}$  phases as well as presence in their structure of the weakly-bound (labile) oxygen causes possibility of their usage as materials for semiconducting chemical sensors of gases, oxidation catalysts of hydrocarbons, electrode materials for high-temperature electrochemical devices (chemical electrical supplies) as well as materials for high-temperature conversion of heat into electrical energy in thermoelectric generators (thermal electrical supplies).

## Table of contents

1. Introduction	1
2. Synthesis and crystal structure	2
2.1. $LnAMe_2O_{5+\delta}$ ( $Ln$ – Y, REE; M – AE, AEE; Me – Cr, Mn, Fe, Co) phases	3
2.2. $LnAMe'Me''O_{5+\delta}$ ( $Ln$ – Y, REE; A – Ba, Sr; Me', Me'' – Mn, Fe, Co, Cu) phases	7
3. Thermal stability and thermal expansion	11
3.1. $LnBaMe_2O_{5+\delta}$ ( $Ln$ – Y, REE; Me – Mn, Fe, Co) phases	11
3.2. $LnBaMe'Me''O_{5+\delta}$ ( $Ln$ – Y, REE; Me', Me'' – Fe, Co, Cu) phases	12
4. Magnetic properties	15
4.1. $LnAMe_2O_{5+\delta}$ ( $Ln$ – Y, REE; A – AE, AEE; Me – Mn, Fe, Co) phases	15
4.2. $LnBaMe'Me''O_{5+\delta}$ ( $Ln$ – Y, REE; Me', Me'' – Fe, Co, Cu) phases	18
5. Electric properties	18
5.1. $LnBaMe_2O_{5+\delta}$ ( $Ln$ – Y, REE; Me – Mn, Fe, Co) phases	19
5.2. $LnBaMe'Me''O_{5+\delta}$ ( $Ln$ – Y, REE; Me', Me'' – Fe, Co, Cu) phases	21
6. Catalytic, sensor, thermoelectric and other properties	24
7. Conclusion	26
8. References	27

## 1. Introduction

Oxides having perovskite ( $ABO_3$ ) or perovskite-like structure possess a number of interesting form scientific point of view and important for practical using properties. The representatives of perovskite family are ferroelectrics (including  $BaTiO_3$  which also possess positive temperature coefficient of resistivity (PTCR) [1]), high-temperature superconductors (HTSC) ( $YBaCu_3O_{7-\delta}$ ,  $Ba(Pb,Bi)O_3$  [2]), proton ( $BaZrO_3$  [3]) and oxygen-ion conducting ( $LaGaO_3$ ,  $LaCoO_3$  [4,5]) solid electrolytes (SE), chemical reactions catalysts [5] and chemical sensors of gases [6,7],  $LaMnO_3$  derivatives which demonstrate colossal magneto-resistive effect (CMR) [8] etc. Recently some perovskites as prospective oxide thermoelectric for high-temperature thermoelectric conversion devices were proposed ( $La(Co,Ni,Ti)O_3$  [9] and  $(Ba,Sr)PbO_3$  [10] ceramics.

Last decades a great interest attempt oxygen-deficient layered  $LnAMe_2O_{5+\delta}$  ( $Ln$  – rare-earth element (REE); A – alkaline element (AE) or alkali-earth element (AEE); Me – 3d- metal) oxides,

which structure from simple perovskite structure owing to arrangement of REE and AE (AEE) ions in their structure is formed. When  $0 < \delta < 1$ , arrangements of REE/AE(AEE) cations in  $LnAMe_2O_{5+\delta}$  phases is accompanied by arrangement of oxygen ions vacancies in their crystal structure (namely in  $-LnO_{\delta-}$  layers).

Perovskite ( $ABO_3$ ) structure can be imagined as three-dimensional frame structure constructed from corner-sharing  $MO_6$  octahedra. The A-cations are located in the holes of this structure and by 12 O anions are coordinated [11]. Layered perovskite-like  $LnAMe_2O_{5+\delta}$  oxides have so-called 0112 or  $YBaFeCuO_5$  structure which had been determined for the first time in [12]. Structure of  $YBaFeCuO_5$  can be described as an ordered oxygen-deficient perovskite which exhibits a great similarity to the  $YBa_2Cu_3O_{7-\delta}$  HTSC structure [2]. The barium of barium and yttrium (REE) ions form planes perpendicular to  $c$  axis, which alternate according to the sequence  $\dots Ba-Y-Ba\dots$ , whereas the sequence  $\dots Ba-Ba-Y-Ba-Ba\dots$  is observed for the  $YBa_2Cu_3O_{7-\delta}$  structure. Moreover, the vacancies of oxygen are located at the same level as the yttrium ions in these structures, so that they both exhibit layers of polyhedral whose cohesion is ensured by yttrium ions. The layers  $[-(Cu,Fe)O_{5-}]_{\infty}$  of  $YBaFeCuO_5$  are themselves built up from double layers of corner-sharing  $CuO_5$  and  $FeO_5$  pyramids, whereas triple polyhedra layers are observed in HTSC  $YBa_2Cu_3O_{7-\delta}$ . In both compounds the barium ions are located inside the layers [12]. So,  $YBaFeCuO_5$  structure can be imagined as sequence of layers  $-Y-(Cu,Fe)O_2-BaO-(Cu,Fe)O_2-Y$ . There are three non-equivalent positions in 0112 structure for oxygen ions: O1 positions in the  $-BaO-$  layers, O2 positions in  $-(Cu,Fe)O_2-$  layers and O3 positions in  $-Y-$  layers (fig. 1). The O3 positions in  $YBaFeCuO_5$  are fully empty (fully occupied by oxygen ion vacancies) but for other 0112 compounds these positions can be partially or fully occupied.

Layered  $LnBaMe_2O_{5+\delta}$  ( $Ln$  – REE;  $Me$  –  $3d$ - metal) compounds demonstrate the phase transition “insulator to metal” ( $YBaMn_2O_6$  [13],  $PrBaCo_2O_{5+\delta}$  [14]) and catalytic activity in reaction of oxidation of hydrocarbons by atmospheric oxygen ( $YBaFeCuO_5$ -based materials [15]). These compounds may be used as materials for semiconducting sensors of gases [6,16], cathodes for intermediate-temperature solid oxide fuel cells (IT SOFC) [17–20], membranes for gas separation (possess high oxygen permeability  $GdBaCo_2O_{5+\delta}$  [19]), thermoelectric materials for high-temperature conversion of heat into electrical energy [21,22].  $LaAMn_2O_{5+\delta}$  ( $A$  – K, Rb, Cs) phases exhibit negative giant magneto-resistance (GMR) [23].

The riches of properties of  $LnAMe_2O_{5+\delta}$  phases are caused by that cations of  $3d$ -metals in their crystal structure can exist in different charge and spin states which strongly depend on radius and charge of  $Ln(A)$  cations, the oxygen non-stoichiometry index ( $\delta$ ) of these phases and also an ordering degree of their oxygen sub-lattice. All the 0112 compounds can be divided in two groups:  $LnAMe_2O_{5+\delta}$  phases which contain only one  $3d$ -metal (layered manganites  $LnBaMn_2O_{5+\delta}$  [13], cobaltites  $LnBaCo_2O_{5+\delta}$  [14, 17–19] etc.) and  $LnAMe'Me''O_{5+\delta}$  phases which B cationic sub-lattice filled by equal quantities of two  $3d$ -metals (layered ferrocuprates  $LnBaFeCuO_{5+\delta}$  [12,16,21], ferrocobaltites  $LnBaFeCoO_{5+\delta}$  [20,22] etc.). Properties of the  $LnAMe'Me''O_{5+\delta}$  layered oxides can depend also on the ordering degree of different B-cations in their crystal structure.

## 2. Synthesis and crystal structure

Usually the  $LnAMe_2O_{5+\delta}$  ( $Ln$  – REE;  $A$  – AE or AEE;  $Me$  –  $3d$ - metal) compounds prepare by ceramic method from binary oxides and carbonates of corresponding metals at conditions depending on the nature of  $3d$ -metals (annealing temperature, oxidizing or reducing atmosphere, thermal prehistory etc.). Alternative method of preparation of  $LnAMe_2O_{5+\delta}$  phases are wet-chemical methods (coprecipitation, sol-gel etc.) which allow to obtain high density ceramics at rather low temperatures.

The 0112 phases are the double perovskites, so their crystal structure is mainly tetragonal with unit cell doubled along  $c$  axis:  $a = b = a_p$ ,  $c = 2a_p$  (1:1:2). In some cases, ordering of oxygen vacancies in the  $-LnO_8-$  layers in  $LnAMe_2O_{5+\delta}$  oxides structure lead to the formation of different types superstructures:  $a < b = a_p$ ,  $c \approx 2a_p$  (1:1:2),  $a = b = \sqrt{2}a_p$ ,  $c = 2a_p$  ( $\sqrt{2}:\sqrt{2}:2$ ),  $a = a_p$ ,  $b > c \approx 2a_p$  (1:2:2), etc (most typical for the layered cobaltites). On the other hand, lowering of the 0112 symmetry sometimes caused by the rotation or tilting of the  $MeO_n$  polyhedra ( $n = 5, 6$ ) with formation of different distorted structures (most pronounced for layered manganites etc.).

## 2.1. $LnAMe_2O_{5+\delta}$ ( $Ln - Y, REE$ ; $A - AE, AEE$ ; $Me - Cr, Mn, Fe, Co$ ) phases

The  $LnACr_2O_{5+\delta}$  ( $Ln - Nd, Gd$ ;  $A - Na, K, Cs, Ba, Sr, Mg$ ) compounds were prepared by ceramic method from  $Nd_2O_3$ ,  $Gd_2O_3$ ,  $Cr_2O_3$ ,  $MgO$  and alkaline and other alkali elements carbonates in air in three stages: annealing at 673–1073 K for 10 h, grinding, then annealing at 1073–1773 K for 20 h and after that low-temperature annealing at 673 K for a long time for homogenization of the samples with oxygen [24].

Oxides of composition  $LaAMn_2O_{5+\delta}$  ( $A - K, Rb, Cs$ ) were prepared by dissolving required quantities of  $A_2CO_3$ ,  $La_2O_3$  and  $Mn_2O_4 \cdot 2H_2O$  in 1:1  $HNO_3$ , evaporating the solution to dryness and annealing the dried mass in air at 1023–1173 K for varying durations. Samples were also synthesized by the citrate method followed by prolonged annealing in oxygen at 1023 K to obtain a high oxygen content in  $LaAMn_2O_{5+\delta}$  ( $A - K, Cs$ ). Single-phase products  $LaAMn_2O_{5+\delta}$  ( $K, Rb$ ) were obtained by reaction at 1173 K for 24 h with one intermittent grinding, while the  $LaCsMn_2O_{5+\delta}$  compound was obtained by reaction at 1073 K for 24 h [23].

Ordered  $LnBaMn_2O_6$  layered perovskites have been prepared in three stages [25]. At first the ceramic samples of  $Ln_{0.50}Ba_{0.50}MnO_3$  ( $Ln - REE$ ) perovskites were prepared using ceramic method. Oxides  $Ln_2O_3$ ,  $Mn_2O_3$  and barium carbonate  $BaCO_3$  were weighed in designed cation relation ( $Ln:Ba:Mn = 1:1:2$ ) and thoroughly ground in an agate mortar by adding of some quantity of ethyl alcohol. The prepared mixtures were pressed as pellets and then annealed in air at 1373 K for 2 h with following grind. The synthesis was carried out in air at 1823 K for 2 h. In order to obtain ceramics with oxygen content close to the stoichiometric one the samples were placed on Pt substrate, annealed in air at 1173 K for 100h and then cooled to the room temperature at a rate of  $100 K \cdot h^{-1}$ . On the second stage the reduced  $LnBaMn_2O_5$  samples were prepared by a topotactic reaction method. The samples were placed in evacuated  $SiO_2$  ampoules with some quantity of metallic Ta as an oxygen getter. Ampoules were exposed at 1173 K for 24 h and then cooled down to the room temperature at a rate of  $100 K \cdot h^{-1}$ . The equation for the reduction chemical reaction is the following:



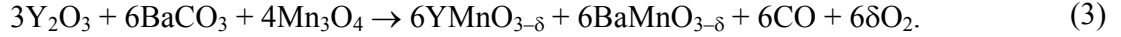
On the third stage the reduced samples were re-oxidized in air at 1173 K for 5 h. The oxidation reaction can be described by an equation:



On the first stage of the synthesis the cubic  $Ln_{0.50}Ba_{0.50}MnO_3$  perovskites with random distribution of  $Ln^{3+}$  and  $Ba^{2+}$  ions on the A site of the perovskite ( $ABO_3$ ) cell. The reducing of the samples lead to the ordering of  $Ln^{3+}$  and  $Ba^{2+}$  ions along  $c$  axis of the manganites structure with formation of the double perovskites of 0112 type ( $LnBaMn_2O_5$ ). Oxidation of the  $LnBaMn_2O_5$  samples by the atmospheric oxygen allow to obtaine from the oxygen-deficient layered  $LnBaMn_2O_5$  compound the oxygen stoichiometric double perovskite  $LnBaMn_2O_6$  [25].

The  $YBaMn_2O_{5+\delta}$  compound is unstable in air so its preparation is carried out in reducing atmospheres [26]. Stoichiometric quantities of the  $Y_2O_3$ ,  $BaCO_3$  and  $Mn_3O_4$  were finely mixed and

grinded in an agate mortar and pestle. The mixture was placed in a tube having atmosphere of flowing high-purity Ar gas (99.9995%, O<sub>2</sub> < 2 ppm) and annealed for a long time at the temperatures of 1193–1373 K. It was found, that reaction proceeds in two stages. On the first stage the formation of YMnO<sub>3-δ</sub> and BaMnO<sub>3-δ</sub> from the initial components is obtained:



On the second stage the formation of YBaMn<sub>2</sub>O<sub>6±δ</sub> from the yttrium (YMnO<sub>3-δ</sub>) and barium manganites (BaMnO<sub>3-δ</sub>) took place [26]:

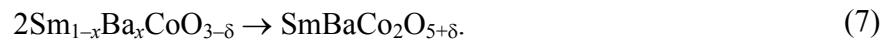


YBaMn<sub>2</sub>O<sub>6±δ</sub> phase can be prepared directly from the YMnO<sub>3-δ</sub> and BaMnO<sub>3-δ</sub> precursors. The formation of YBaMn<sub>2</sub>O<sub>6±δ</sub> on the reaction (4) is finished after annealing of precursors mixture in an flowing Ar at 1273 K for 65 h [26].

The LnBaFe<sub>2</sub>O<sub>5+δ</sub> compounds after unstable in air so their synthesis should be performed in a strongly reducing atmosphere. The preparation method of these compound can be featured on an DyBaFe<sub>2</sub>O<sub>5+δ</sub> example [27]. Amorphous precursor for synthesis of DyBaFe<sub>2</sub>O<sub>5+δ</sub> was obtained from Dy<sub>2</sub>O<sub>3</sub>, metallic Fe and BaCO<sub>3</sub> by liquid mixing in a citrate melt. Calcination was performed at 1173 K in an atmosphere of Ar, H<sub>2</sub> and H<sub>2</sub>O having log(*p*<sub>O<sub>2</sub></sub>, bar) ≈ -16; yielding a single-phase powder. The master sample was sintered at 1273 K under log(*p*<sub>O<sub>2</sub></sub>, bar) ≈ -15,2. The equilibrated samples were quenched into a metal container filled with high-purity Ar (< 2 ppm O<sub>2</sub>, dried over a P<sub>2</sub>O<sub>5</sub> decassant) [27].

Ceramic polycrystalline samples of LnBaCo<sub>2</sub>O<sub>5+δ</sub> had been prepared using the conventional solid-state reaction method. Stoichiometric amounts of Ln<sub>2</sub>O<sub>3</sub>, BaCO<sub>3</sub> and CoO had been thoroughly mixed and then calcined at 1173 K for 12 h in air. The calcined powder had been re-ground and sintered at 1273 k for 15 h in air. The final step consisted of re-grinding these sintered powder, pressing into pellets and then sintering in air at 1373 K for 24 h [28].

SmBaCo<sub>2</sub>O<sub>5+δ</sub> compound was also synthesized via combustion process combined with a solid state reaction method, using undissolved Co<sub>3</sub>O<sub>4</sub> as a starting material [29]. The flow chart is given in fig. 2. Ba(CH<sub>3</sub>COO)<sub>2</sub>, Co<sub>3</sub>O<sub>4</sub> and Sm<sub>2</sub>O<sub>3</sub> served as the raw materials for the necessary metal ions. First, Sm<sub>2</sub>O<sub>3</sub> was dissolved in HNO<sub>3</sub>, than Ba(CH<sub>3</sub>COO)<sub>2</sub> and Co<sub>3</sub>O<sub>4</sub> were added into Sm<sup>3+</sup> solution under stir. Subsequently, citric acid with molar ratios of soluble metal: citric acid of 1:1,5 was added and pH value was adjusted to about 7 with ammonia. The suspension was heated and stirred continuously at 353–363 K till to ignition and combustion, getting as-prepared powders. And subsequently as-prepared powders were calcined at various temperatures (923–1173 K) in air to yield th expected powders [29]. According to [29], the formation of SmBaCo<sub>2</sub>O<sub>5+δ</sub> proceeds in three stages (5–7):



On the first stage (5) the formation the barium cobaltite BaCoO<sub>3-δ</sub> was occurred, which react with the Sm<sub>2</sub>O<sub>3</sub> and Co<sub>3</sub>O<sub>4</sub> on the second stage (6) with formation of perovskite solid solution Sm<sub>1-x</sub>Ba<sub>x</sub>CoO<sub>3-δ</sub>. On the third stage (7) Sm<sub>1-x</sub>Ba<sub>x</sub>CoO<sub>3-δ</sub> solid solution (random distribution of Sm<sup>3+</sup> and Ba<sup>2+</sup> ions) transforms into layered oxygen deficient double perovskite SmBaCo<sub>2</sub>O<sub>5+δ</sub> (Sm<sup>3+</sup> and Ba<sup>2+</sup> ions arranged along the c axis).

In [19] the LnBaCo<sub>2</sub>O<sub>5+δ</sub> (Ln = La, Y, Pr, Nd, Sm and Gd) composite oxides were synthesized via combined EDTA–citrate complexing sol–gel process. Ba(NO<sub>3</sub>)<sub>2</sub>, Co(NO<sub>3</sub>)<sub>2</sub>·xH<sub>2</sub>O and Ln(NO<sub>3</sub>)<sub>3</sub>·xH<sub>2</sub>O

(all reagent grade) served as the raw materials for the necessary metal ions. Separate 1 M solutions of the nitrates were prepared, and their precise concentrations were determined by titration with EDTA. From these solutions, solutions were prepared with molar ratios of total metal ions:EDTA: citric acid of 1:1:2, and their pH values were adjusted to ~6 with NH<sub>4</sub>OH. The solutions were heated continuously at 363 K until sufficient water had evaporated that a transparent purple gel was obtained. This gel was pre-fired at 523 K and subsequently calcinated at various temperatures for 5 h under an air atmosphere to yield desired oxide powder products. These oxide powders were pressed into disks under approximately 1.5·10<sup>8</sup> Pa hydraulic pressure. The resulting green disks were further sintered at 1373–1423 K for 2–5 h in air. During this time, the heating and cooling rates were controlled at 1–2 K·min<sup>-1</sup>. The sintered ceramics had relative density within ≈96–99% [19].

$LnACr_2O_{5+\delta}$  ( $Ln$  – Nd, Gd;  $A$  – Na, K, Cs, Ba, Sr, Mg) compounds had tetragonal structure with lattice constants  $a = 10.74$ – $10.93$  Å,  $c = 15.94$ – $19.86$  Å (table 1). The values of the lattice constants of  $LnACr_2O_{5+\delta}$  oxides show that they are characterized with superstructures of  $(2\sqrt{2}:2\sqrt{2}:4)$  type:  $a = b = 2\sqrt{2}a_p$ ,  $c = 4a_p$ . It is interesting, that values of  $c$  parameter of  $LnACr_2O_{5+\delta}$  phases depend on the nature of lanthanide and alkaline/alkali earth metals larger than values of  $a$  parameters. This fact show that increasing of  $Ln^{3+}$  or  $A^+(A^{2+})$  ionic radius lead to the expansion of  $LnACr_2O_{5+\delta}$  phases unit cell along  $c$  axis and slightly involve on the inter-atomic distances in the basal plane of these oxides crystal structure.

Table 1. Structure and lattice constants of  $LnAME_2O_{5+\delta}$  ( $Ln$  – Y, REE;  $A$  – AE, AEE;  $Me$  – Cr, Mn, Fe, Co) phases

Compound	Structure*	Space group	$a$ , Å ( $\alpha$ , °)	$b$ , Å ( $\beta$ , °)	$c$ , Å ( $\gamma$ , °)	$a_p$ , Å**	Ref.
1	2	3	4	5	6	7	8
NdNaCr <sub>2</sub> O <sub>5</sub>	T	–	10.88	–	19.83	4.186	[24]
NdKCr <sub>2</sub> O <sub>5</sub>	T	–	10.87	–	19.86	4.186	[24]
NdCsCr <sub>2</sub> O <sub>5</sub>	T	–	10.93	–	19.60	4.183	[24]
GdNaCr <sub>2</sub> O <sub>5</sub>	T	–	10.78(1)	–	15.94(6)	3.868	[30]
GdKCr <sub>2</sub> O <sub>5</sub>	T	–	10.74(1)	–	17.73(3)	3.998	[30]
GdCsCr <sub>2</sub> O <sub>5</sub>	T	–	10.85(6)	–	19.83(3)	4.178	[30]
NdMgCr <sub>2</sub> O <sub>5.5</sub>	T	–	10.87	–	17.68	4.027	[24]
GdBaCr <sub>2</sub> O <sub>5.5</sub>	T	–	10.77	–	17.90	4.018	[31]
GdSrCr <sub>2</sub> O <sub>5.5</sub>	T	–	10.79	–	16.72	3.933	[32]
GdMgCr <sub>2</sub> O <sub>5.5</sub>	T	–	10.79	–	16.54	3.919	[33]
LaKMn <sub>2</sub> O <sub>5.53</sub>	T	–	7.745(1)	–	7.020(2)	3.748	[23]
LaRbMn <sub>2</sub> O <sub>5.53</sub>	T	–	7.773(1)	–	7.149(1)	3.780	[23]
LaCsMn <sub>2</sub> O <sub>5.6</sub>	O	–	5.511(2)	5.468(3)	7.311(4)	3.805	[23]
LaKMn <sub>2</sub> O <sub>5</sub>	T	–	7.781(5)	–	21.133(2)	4.308	[39]
YBaMn <sub>2</sub> O <sub>5</sub>	T	$P4/mmm$	3.9204(1)	–	7.6614(3)	3.890	[34]
YBaMn <sub>2</sub> O <sub>5.6(2)</sub>	T	–	3.9221(3)	–	7.6648(8)	3.892	[35]
YBaMn <sub>2</sub> O <sub>5</sub>	T	$P4/mmm$	5.547	–	7.649	3.889	[36]
YBaMn <sub>2</sub> O <sub>6</sub>	Tr	$P\bar{1}$	5.51974 (8) (90.017(2))	5.51379(8) (90.280(1))	7.60319(10) (90.106(1))	3.868	[37]
YBaMn <sub>2</sub> O <sub>6</sub>	M	$P2$	5.5181(4)	5.5142(4) (90.267(4))	7.6443(3)	3.874	[13]
YBaMn <sub>2</sub> O <sub>6</sub>	M( $pT$ )	–	3.901(9)	3.898(1) (90,2(1))	7.602(2)	3.869	[38]
LaBaMn <sub>2</sub> O <sub>5.5</sub>	O	$Ammm$	3.8564(2)	8.1883(4)	15.4734(8)	3.938	[40]
LaBaMn <sub>2</sub> O <sub>5.5</sub>	C	$Pm\bar{3}m$	11.039	–	–	3.680	[41]
LaCaMn <sub>2</sub> O <sub>5.5</sub>	C	$Pm\bar{3}m$	10.890	–	–	3.630	[41]
PrBaMn <sub>2</sub> O <sub>6</sub>	T	–	3.900	–	7.775	3.896	[25]
NdBaMn <sub>2</sub> O <sub>5.5</sub>	C	$Pm\bar{3}m$	11.007	–	–	3.669	[41]
NdBaMn <sub>2</sub> O <sub>6</sub>	T	–	3.899	–	7.756	3.892	[25]

1	2	3	4	5	6	7	8
NdCaMn <sub>2</sub> O <sub>5.5</sub>	C	<i>Pm3m</i>	10.789	–	–	3.596	[41]
SmBaMn <sub>2</sub> O <sub>6</sub>	T	–	3.900	–	7.712	3.885	[25]
EuBaMn <sub>2</sub> O <sub>6</sub>	O	–	3.917	3.835	7.764	3.878	[25]
GdBaMn <sub>2</sub> O <sub>5.5</sub>	T	–	10.957	–	31.684	3.903	[42]
GdBaMn <sub>2</sub> O <sub>6</sub>	T	–	3.901	–	7.651	3.876	[25]
TbBaMn <sub>2</sub> O <sub>6</sub>	T	–	3.899	–	7.645	3.873	[25]
LaBaFe <sub>2</sub> O <sub>5.5</sub>	T	–	11.13	–	19.01	4.191	[43]
LaSrFe <sub>2</sub> O <sub>5.5</sub>	T	–	10.81	–	16.38	3.911	[43]
LaCaFe <sub>2</sub> O <sub>5.5</sub>	T	–	11.15	–	19.00	4.195	[43]
LaMgFe <sub>2</sub> O <sub>5.5</sub>	T	–	11.06	–	17.05	4.024	[43]
NdBaFe <sub>2</sub> O <sub>5.467(1)</sub>	T	–	3.9498(3)	–	7.7638(9)	3.927	[44]
SmBaFe <sub>2</sub> O <sub>5.346(2)</sub>	T	–	3.9433(3)	–	7.7143(8)	3.914	[44]
SmBaFe <sub>2</sub> O <sub>5.646(2)</sub>	T	–	3.9272(6)	–	7.8237(28)	3.922	[45]
DyBaFe <sub>2</sub> O <sub>5</sub>	O	<i>Pmmm</i>	3.93855(1)	3.92433(1)	7.57344(1)	3.883	[27]
YbBa <sub>2</sub> Fe <sub>2</sub> O <sub>5.5</sub>	O	–	10.74(1)	10.99(1)	17.16(2)	3.985	[46]
YbSrFe <sub>2</sub> O <sub>5.5</sub>	O	–	10.74(1)	10.93(1)	16.64(5)	3.937	[46]
YBaCo <sub>2</sub> O <sub>5.19</sub>	T	–	3.878	–	7.495	3.834	[47]
YBaCo <sub>2</sub> O <sub>5.30</sub>	T	–	3.873	–	7.503	3.832	[48]
YBaCo <sub>2</sub> O <sub>5.41(7)</sub>	O	<i>Pmmm</i>	3.854(0)	3.846(7)	7.485(0)	3.814	[19]
LaBaCo <sub>2</sub> O <sub>5.90</sub>	C	–	3.885	–	–	3.885	[49]
LaBaCo <sub>2</sub> O <sub>5.24(1)</sub>	C	<i>Pm3m</i>	3.886(1)	–	–	3.886	[28]
LaBaCo <sub>2</sub> O <sub>5.80(5)</sub>	O	<i>Pmmm</i>	3.898(1)	3.891(5)	7.718(2)	3.883	[19]
PrBaCo <sub>2</sub> O <sub>5.53(1)</sub>	O	<i>Pmmm</i>	3.910(4)	7.830(6)	7.635(3)	3.881	[28]
PrBaCo <sub>2</sub> O <sub>5.77</sub>	O	<i>Pmmm</i>	3.8981(1)	7.7069(2)	7.6354(2)	3.856	[51]
PrBaCo <sub>2</sub> O <sub>5.5</sub>	O	<i>Pmmm</i>	3.9049(1)	7.8733(2)	7.6084(2)	3.882	[53]
PrBaCo <sub>2</sub> O <sub>5.48</sub>	O	<i>Pmmm</i>	3.9068(1)	7.8807(1)	7.6145(2)	3.884	[14]
PrBaCo <sub>2</sub> O <sub>5.77(4)</sub>	O	<i>Pmmm</i>	3.896(4)	3.890(0)	7.612(7)	3.864	[19]
NdBaCo <sub>2</sub> O <sub>5.62</sub>	T	–	3.900	–	3.802	3.867	[49]
NdBaCo <sub>2</sub> O <sub>5.57(8)</sub>	O	<i>Pmmm</i>	3.903(8)	7.821(3)	7.612(6)	3.873	[28]
NdBaCo <sub>2</sub> O <sub>5.69</sub>	O	<i>Pmmm</i>	3.90124(7)	7.8156(2)	7.60671(9)	3.871	[57]
NdBaCo <sub>2</sub> O <sub>5.69(0)</sub>	O	<i>Pmmm</i>	3.889(1)	3.872(7)	7.599(3)	3.853	[19]
SmBaCo <sub>2</sub> O <sub>5.39(4)</sub>	O	<i>Pmmm</i>	3.892(2)	7.842(7)	7.567(4)	3.865	[28]
SmBaCo <sub>2</sub> O <sub>5.68(5)</sub>	O	<i>Pmmm</i>	3.885(2)	3.866(0)	7.569(2)	3.845	[19]
EuBaCo <sub>2</sub> O <sub>5.39(4)</sub>	O	<i>Pmmm</i>	3.891(7)	7.847(7)	7.558(7)	3.864	[28]
EuBaCo <sub>2</sub> O <sub>5.49</sub>	O	<i>Pmmm</i>	3.8823(1)	7.8187(2)	7.5481(2)	3.855	[50]
GdBCo <sub>2</sub> O <sub>5.43(3)</sub>	O	<i>Pmmm</i>	3.878(5)	7.836(4)	7.544(2)	3.856	[28]
GdBaCo <sub>2</sub> O <sub>5.45</sub>	O	<i>Pmmm</i>	3.8735(1)	7.8183(1)	7.5300(1)	3.8487	[54]
GdBaCo <sub>2</sub> O <sub>5.66(7)</sub>	O	<i>Pmmm</i>	3.861(9)	3.860(4)	7.519(8)	3.827	[19]
TbBaCo <sub>2</sub> O <sub>5.60</sub>	O	–	3.886	3.860	3.737	3.827	[49]
TbBaCo <sub>2</sub> O <sub>5.41(0)</sub>	O	<i>Pmmm</i>	3.877(4)	7.833(0)	7.533(4)	3.853	[28]
TbBaCo <sub>2</sub> O <sub>5.5</sub>	O	<i>Pmmm</i>	3.9065(1)	7.7371(3)	7.5152(4)	3.844	[55]
DyBaCo <sub>2</sub> O <sub>5.20(8)</sub>	O	<i>Pmmm</i>	3.891(4)	7.770(6)	7.533(6)	3.847	[28]
DyBaCo <sub>2</sub> O <sub>5.46</sub>	O	<i>Pmmm</i>	3.860(1)	7.811(1)	7.506(1)	3.839	[52]
HoBaCo <sub>2</sub> O <sub>5.49(1)</sub>	O	<i>Pmmm</i>	3.8698(1)	7.8167(1)	7.5179(1)	3.845	[56]
HoBaCo <sub>2</sub> O <sub>5.20(9)</sub>	O	<i>Pmmm</i>	3.883(9)	7.754(2)	7.508(7)	3.838	[28]
HoBaCo <sub>2</sub> O <sub>5.36</sub>	O	<i>Pmmm</i>	3.873(1)	7.751(1)	7.498(2)	3.832	[52]

\* C – cubic, T – tetragonal, pT – pseudotetragonal, O – orthorhombic, M – Monoclinic, Tr – triclinic

\*\* Calculated using literature data

The LaAMn<sub>2</sub>O<sub>5+δ</sub> (A – K, Rb, Cs) phases adopt an ordered superstructure of perovskite. The LaKMn<sub>2</sub>O<sub>5+δ</sub> and LaRbMn<sub>2</sub>O<sub>5+δ</sub> are tetragonal ( $a \approx 7.75 \text{ \AA}$ ,  $c \approx 7.10 \text{ \AA}$ ) but the LaCsMn<sub>2</sub>O<sub>5+δ</sub> compound is orthorhombic ( $a = 5.511 \text{ \AA}$ ,  $b = 5.468 \text{ \AA}$ ,  $c = 7.311 \text{ \AA}$ ) indicating (2:2:2) ( $a = b > c = 2a_p$ )

and ( $\sqrt{2}:\sqrt{2}:2$ ) ( $a > b \approx \sqrt{2}a_p$ ,  $c = 2a_p$ ) superstructures, respectively. Lattice constants of  $\text{LaAMn}_2\text{O}_{5+\delta}$  compounds increase at alkaline element ionic radius increasing (table 1).

$\text{LnBaMn}_2\text{O}_{5+\delta}$  compounds had a tetragonal structure with supercell of (1:1:2) type ( $a = b = 2a_p$ ,  $c = 2a_p$ ) [25,34,35], though some authors describe their as cubic ( $a = 3a_p$ ) [41] or tetragonal with superstructure of ( $2\sqrt{2}:2\sqrt{2}:8$ ) type ( $a = b = 2\sqrt{2}a_p$ ,  $c = 8a_p$ ) [42] (table 1). According to [40],  $\text{LaBaMn}_2\text{O}_{5.5}$  adopt orthorhombic structure (sp. gr. *Ammm*,  $a = 3.86 \text{ \AA}$ ,  $b = 8.19 \text{ \AA}$ ,  $c = 15.47 \text{ \AA}$ ) with superstructure of (1:2:4) type ( $a = a_p$ ,  $b = 2a_p$ ,  $c = 4a_p$ ).  $\text{YBaMn}_2\text{O}_6$  at a room temperature has monoclinic structure (sp.gr. *P2*,  $Z = 2$ ,  $a = 5.5181(4) \text{ \AA}$ ,  $b = 5.5142(4) \text{ \AA}$ ,  $c = 7.6443(3) \text{ \AA}$ ,  $\beta = 90.267(4)^\circ$ ) with superstructure of ( $\sqrt{2}:\sqrt{2}:2$ ) type ( $a > b \approx \sqrt{2}a_p$ ,  $c = 2a_p$ ), which transforms at 520 K into triclinic one (sp. gr. *P1*,  $Z = 2$ ,  $a = 5.4948(15) \text{ \AA}$ ,  $b = 5.4920(14) \text{ \AA}$ ,  $c = 7.7174(4) \text{ \AA}$ ,  $\alpha = 89.804(20)^\circ$ ,  $\beta = 90.173(20)^\circ$ ,  $\gamma = 91.160(4)^\circ$ ) [13]. In a whole, lattice constants of  $\text{LnBaMn}_2\text{O}_{5+\delta}$  slightly depend on the  $\text{Ln}^{3+}$  ionic radii (see fig. 3a), nevertheless the linear decreasing of the unit cell volume of  $\text{LnBaMn}_2\text{O}_{5+\delta}$  oxides at decreasing of  $R_{\text{Ln}^{3+}}$  had been detected [25].

Ferrites  $\text{LnAFe}_2\text{O}_{5+\delta}$  ( $\text{Ln} - \text{REE}$ ;  $\text{A} - \text{AEE}$ ) adopt tetragonal or orthorhombic structure with superstructure of (1:1:2) ( $a > b \approx a_p$ ,  $c = 2a_p$ ) or ( $2\sqrt{2}:2\sqrt{2}:4$ ) type ( $a > b \approx 2\sqrt{2}a_p$ ,  $c = 4a_p$ ) (table 1). They lattice constants, as a rule, decreased at decreasing of REE or AEE ionic radii (table 1). Values of the unit cell parameters of  $\text{LnBaFe}_2\text{O}_{5+\delta}$  compounds strongly depend on their oxygen non-stoichiometry. As can be seen from the fig. 4, the  $\text{SmBa}_2\text{Fe}_2\text{O}_{5+\delta}$  structure is orthorhombic at low  $\delta$  ( $\delta < 0.05$ ) and transform into tetragonal at  $\delta > 0.05$ . The  $a$  parameters of  $\text{SmBaFe}_2\text{O}_{5+\delta}$  decreases but  $c$  parameter increases when  $\delta$  increases, that resulting in the increasing of tetragonal distortion degree of  $\text{SmBaFe}_2\text{O}_{5+\delta}$  compounds with  $\delta$  increasing.

The  $\text{LnBaCoO}_{5+\delta}$  ( $\text{Ln} - \text{REE}$ ) layered cobaltites adopt cubic structure for  $\text{Ln} = \text{La}$  [28,49], tetragonal one for  $\text{Ln} = \text{Y}$  with superstructure of (1:1:2) type ( $a = b = a_p$ ,  $c = 2a_p$ ) [47,48] and orthorhombic one for other lanthanides with superstructure of (1:1:2) type ( $a > b \approx a_p$ ,  $c = 2a_p$ ) [19] or (1:2:2) type ( $a = a_p$ ,  $b = 2a_p$ ,  $c = 2a_p$ ) [14,28,50–57] due to ordering of oxygen ion vacancies in their structure (table 1). According to [49],  $\text{NdBaCo}_2\text{O}_{5.62}$  and  $\text{TbBaCo}_2\text{O}_{5.60}$  had no superstructure and are tetragonal and orthorhombic perovskites, respectively. The lattice constants of the  $\text{LnBaCoO}_{5+\delta}$  phases decrease at  $R_{\text{Ln}^{3+}}$  decreasing which most pronounced for  $c$  parameters (fig. 3b). So, increasing of the lanthanide ionic radii in  $\text{LnBaCoO}_{5+\delta}$  leads to the preferential expansion of the crystal structure along  $c$  axis (perpendicular to the  $-\text{CoO}_2-$  layers).

## 2.2. $\text{LnAMe}'\text{Me}''\text{O}_{5+\delta}$ ( $\text{Ln} - \text{Y}$ , $\text{REE}$ ; $\text{A} - \text{Ba}$ , $\text{Sr}$ ; $\text{Me}'$ , $\text{Me}'' - \text{Mn}$ , $\text{Fe}$ , $\text{Co}$ , $\text{Cu}$ ) phases

$\text{YBaMnCoO}_{5+\delta}$  compound had been prepared from amorphous precursors obtained by liquid mixing in melted citric acid monohydrate. Standardized  $\text{Y}_2\text{O}_3$  had been dry-mixed with the citric acid and dissolved upon melting assisted by a small amount of  $\text{H}_2\text{O}$ . Manganese and cobalt had been dissolved in dilute  $\text{HNO}_3$  and gradually added into the melt, while the mixture had been warmed up until nitrose gases ceased to develop. After cooling below 373 K, redistilling  $\text{H}_2\text{O}$  had been added and  $\text{BaCO}_3$  had been dissolved. Resulting clear viscous melt had been decomposed into an organic-based xerogel at 453 K, powdered in a vibration mill, and incinerated in air for 5 days in a tall porcelain crucible at 673 K. The crucible had been covered with a lid for the first 24 h. Such a procedure yielded a dense, highly sinterable, X-ray amorphous nanopowders of oxides–hydroxides–carbonates. This precursor had been converted to a single-phase oxide product already after 12 h of calcinations at 1133 K in flowing atmosphere of  $\text{Ar}/\text{H}_2$  ( $\log(p_{\text{O}_2}) = -14.85$ ). The powder obtained from calcinations process had been pressed into pellets and sintered for 24 h at 1313 K in argon (99.999% Ar; nominal content 2 ppm  $\text{O}_2$  and 3 ppm  $\text{H}_2\text{O}$ ) dried by passing through a column containing  $\text{P}_2\text{O}_5$  [58].

The other  $LnBaMe'Me''O_{5+\delta}$  ( $Ln - Y, REE; Me', Me'' - Fe, Co, Cu$ ) compounds and  $YSrFeCuO_5$  were prepared using conventional ceramic method from corresponding oxides and carbonates in air at 1173–1473 K for a long time with a maximal temperature 1473, 1273 and 1183–1233 K for  $LnBaFeCoO_{5+\delta}$  [21,59],  $LnBaFeCuO_{5+\delta}$  [60] and  $LnBaCoCuO_{5+\delta}$  [61] phases respectively.

The  $YBaCoCuO_5$  sample had been also prepared from liquid-mixed citrate precursors [62]. Reagent grade  $Y_2O_3$ ,  $BaCO_3$  and  $CuCO_3 \cdot Cu(OH)_2 \cdot 0.5H_2O$  had been dissolved in boiling citric acid, and  $CoC_2O_4 \cdot 4H_2O$  dissolved in hot concentrated  $HNO_3$  had been added to this solution. The clear citrate gel was then dehydrated at 453 K and the resulting product had been finely milled and incinerated in air at 723 K. The pressed powders had been fired four times for 60 h at 1223 K in an atmosphere of purified oxygen and re-homogenized after each firing. The last firing cycle had been followed by 30 h of annealing at 643 K in the same oxygen atmosphere [62].

$YBaMnCoO_{5.004}$  had tetragonal structure (sp.gr.  $P4/mmm$ ,  $a = b = 3.89198(0) \text{ \AA}$ ,  $c = 7.59783(2) \text{ \AA}$ ) with superstructure of (1:1:2) type ( $a = b = 2a_p$ ,  $c = 2a_p$ ) and its crystal structure did not change in temperature interval 10–460 K [58].

The  $LnBaMe'Me''O_{5+\delta}$  ( $Ln - REE; Me', Me'' - Fe, Co, Cu$ ) compounds adopt cubic structure for  $Ln = La$  due to the random distribution on the A site of perovskite ( $ABO_3$ ) cell and tetragonal one (superstructure of (1:1:2) type ( $a = b = a_p$ ,  $c = 2a_p$ )) for other compounds (table 2, fig. 5).

Table 2. Structure and lattice constants of  $LnAme'Me''O_{5+\delta}$  ( $Ln - Y, REE; A - Ba, Sr; Me - Mn, Fe, Co$ ) phases

Compound	Structure*	Space group	$a, \text{ \AA}$	$b, \text{ \AA}$	$c, \text{ \AA}$	$a_p, \text{ \AA}^{**}$	Ref.
1	2	3	4	5	6	7	8
$YBaMnCoO_5$	T	$P4/mmm$	3.89198(0)	–	7.59783(2)	3.866	[58]
$YBaFeCoO_{5.25}$	T	$P4/mmm$	3.9029(23)	–	7.5538697)	3.860	[59]
$LaBaFeCoO_{5.97}$	C	$Pm3m$	3.9085(10)	–	–	3.909	[63]
$PrBaFeCoO_{5.79}$	T	$P4/mmm$	3.918(2)	–	7.725(6)	3.899	[64]
$NdBaFeCoO_{5.65}$	T	$P4/mmm$	3.909	–	7.695	3.888	[21]
$SmBaFeCoO_{5.37}$	T	$P4/mmm$	3.908	–	7.662	3.882	[21]
$GdBaFeCoO_{5.37}$	T	$P4/mmm$	3.908	–	7.613	3.874	[21]
$TbBaFeCoO_{5.31}$	T	$P4/mmm$	3.9000(21)	–	7.5922(65)	3.865	[59]
$DyBaFeCoO_{5.34}$	T	$P4/mmm$	3.8973(21)	–	7.5679(62)	3.859	[59]
$HoBaFeCoO_{5.28}$	T	$P4/mmm$	3.8970(24)	–	7.5507(73)	3.856	[59]
$YBaCoCuO_5$	T	$P4/mmm$	3.8679(1)	–	7.5674(2)	3.840	[62]
$YBaCoCuO_{5+\delta}$	T	–	3.874(5)	–	7.571(10)	3.844	[65]
$YBaCoCuO_{4.98}$	T	$P4/mmm$	3.867(2)	–	7.567(7)	3.839	[66]
$LaBaCoCuO_{5.2}$	T	$P4/mmm$	3.9352(3)	–	19.538(2)	3.925	[67]
$LaBaCoCuO_{5.6}$	O	$Pmmm$	3.9223(3)	3.9360(3)	11.7073(8)	3.920	[68]
$LaBaCoCuO_{5.62}$	C	$Pm3m$	3.9228(12)	–	–	3.923	[63]
$PrBaCoCuO_{5.30}$	T	$P4/mmm$	3.915(2)	–	7.685(8)	3.891	[64]
$NdBaCoCuO_{5.21}$	T	$P4/mmm$	3.906(2)	–	7.648(7)	3.878	[61]
$SmBaCoCuO_{5.06}$	T	$P4/mmm$	3.904(2)	–	7.609(6)	3.871	[61]
$GdBaCoCuO_{5.02}$	T	$P4/mmm$	3.891(2)	–	7.592(6)	3.859	[61]
$DyBaCoCuO_{5.01}$	T	$P4/mmm$	3.872(2)	–	7.562(7)	3.841	[66]
$HoBaCoCuO_{5.01}$	T	$P4/mmm$	3.867(2)	–	7.554(5)	3.837	[69]
$YBaFeCuO_{5.02}$	T	$P4mm$	3.867	–	7.656	3.854	[12]
$YBaFeCuO_{5+\delta}$	T	–	3.8719(9)	–	7.663(2)	3.858	[70]
$YBaFeCuO_{5+\delta}$	T	–	3.872(5)	–	7.681(10)	3.861	[65]
$YBaFeCuO_{5.03}$	T	–	3.878	–	7.672	3.864	[71]
$YBaFeCuO_5$	T	$P4/mmm$	3.8740(2)	–	7.6676(5)	3.861	[72]
$YBaFeCuO_{5+\delta}$	T	$P4mm$	3.8707(2)	–	7.6711(4)	3.859	[73]
$YBaFeCuO_{5.17}$	T	$P4/mmm$	3.8796(5)	–	7.6653(7)	3.864	[74]
$YBaFeCuO_{5.08}$	T	$P4mm$	3.867(7)	–	7.661(5)	3.855	[75]
$YBaFeCuO_5$	T	$P4/mmm$	3.8736(2)	–	7.6637(3)	3.860	[76]

1	2	3	4	5	6	7	8
YBaFeCuO <sub>5.04</sub>	T	<i>P4/mmm</i>	3.865	–	7.656	3.853	[60]
YSrFeCuO <sub>5+δ</sub>	T	<i>P4/mmm</i>	3.8317(1)***	–	7.6076(4)***	3.822	[77]
LaBaFeCuO <sub>5.68</sub>	C	–	3.9256(6)	–	–	3.926	[78]
LaBaFeCuO <sub>5.47</sub>	C	<i>Pm3m</i>	3.924	–	–	3.924	[60]
LaBaFeCuO <sub>5+δ</sub>	C	<i>Pm3m</i>	3.9250(2)	–	–	3.925	[79]
LaBaFeCuO <sub>5+δ</sub>	O	<i>Immm</i>	5.5604(1) <sup>#</sup>	5.5537(1) <sup>#</sup>	7.8163(3) <sup>#</sup>	3.922	[80]
PrBaFeCuO <sub>5.35</sub>	T	–	3.923	–	7.759	3.908	[71]
PrBaFeCuO <sub>5.28</sub>	T	<i>P4/mmm</i>	3.921	–	7.756	3.907	[60]
PrBaFeCuO <sub>5.26(4)</sub>	T	<i>P4/mmm</i>	3.9260(1)	–	7.7669(7)	3.912	[81]
NdBaFeCuO <sub>5.25</sub>	T	–	3.917	–	7.745	3.902	[71]
NdBaFeCuO <sub>5.17</sub>	T	<i>P4mm</i>	3.911(8)	–	7.733(0)	3.896	[75]
NdBaFeCuO <sub>5.12</sub>	T	<i>P4/mmm</i>	3.912	–	7.737	3.897	[60]
SmBaFeCuO <sub>5.03</sub>	T	–	3.906	–	7.714	3.890	[71]
SmBaFeCuO <sub>5.12</sub>	T	<i>P4mm</i>	3.902(3)	–	7.715(9)	3.887	[75]
SmBaFeCuO <sub>5.08</sub>	T	<i>P4/mmm</i>	3.896	–	7.706	3.882	[60]
EuBaFeCuO <sub>5.02</sub>	T	–	3.899	–	7.705	3.883	[71]
EuBaFeCuO <sub>5.08</sub>	T	<i>P4/mmm</i>	3.904	–	7.708	3.887	[60]
GdBaFeCuO <sub>5.11</sub>	T	<i>P4mm</i>	3.892(5)	–	7.691(6)	3.876	[75]
GdBaFeCuO <sub>5.08</sub>	T	<i>P4/mmm</i>	3.895	–	7.693	3.879	[60]
TbBaFeCuO <sub>5.05</sub>	T	<i>P4/mmm</i>	3.880	–	7.683	3.867	[60]
DyBaFeCuO <sub>5.11</sub>	T	<i>P4mm</i>	3.876(3)	–	7.668(0)	3.862	[75]
DyBaFeCuO <sub>5.04</sub>	T	<i>P4/mmm</i>	3.874	–	7.668	3.861	[60]
HoBaFeCuO <sub>5.05</sub>	T	<i>P4/mmm</i>	3.870	–	7.653	3.855	[60]
ErBaFeCuO <sub>5.04</sub>	T	<i>P4/mmm</i>	3.872	–	7.656	3.857	[60]
TmBaFeCuO <sub>5.07</sub>	T	<i>P4mm</i>	3.860(0)	–	7.656(7)	3.849	[75]
TmBaFeCuO <sub>5.06</sub>	T	<i>P4/mmm</i>	3.867	–	7.660	3.855	[60]
TmBaFeCuO <sub>4.98</sub>	T	<i>P4mm</i>	3.7812(2)**	–	7.4854(4)**	3.768	[82,83]
YbBaFeCuO <sub>5.00</sub>	T	–	3.857	–	7.641	3.845	[71]
YbBaFeCuO <sub>5.03</sub>	T	<i>P4/mmm</i>	3.851	–	7.637	3.840	[60]
LuBaFeCuO <sub>5.01</sub>	T	–	3.855	–	7.629	3.841	[71]
LuBaFeCuO <sub>5.08</sub>	T	<i>P4mm</i>	3.851(9)	–	7.639(3)	3.840	[75]
LuBaFeCuO <sub>5.05</sub>	T	<i>P4/mmm</i>	3.861	–	7.652	3.849	[60]
LuBaFeCuO <sub>5.01</sub>	T	<i>P4mm</i>	3.774(1)	–	7.474(2)	3.761	[82,83]
LuBaFeCuO <sub>5+δ</sub>	T	<i>P4mm</i>	3.850	–	7.637	3.839	[84]

\* *C* – cubic, *T* – tetragonal, *O* – orthorhombic

\*\* Calculated using literature data

\*\*\* *T* = 2 K.

<sup>#</sup> *T* = 15 K.

However, neutron diffraction [68] and high-resolution electron microscopy [67] discovered superstructure formation in LaBaCoCuO<sub>5+δ</sub> on account vacancy ordering with formation of superstructure (1:1:3) type ( $a < b \approx a_p$ ,  $c \approx 3a_p$ ) (sp. gr. *Pmmm*) for  $\delta = 0.60$  [68] and (1:1:5) type ( $a = a_p$ ,  $c = 5a_p$ ) (sp. gr. *P4/mmm*) for  $\delta = 0.20$  [67].

Lattice constants of the LnBaMe'Me''O<sub>5+δ</sub> (*Ln* – REE; Me', Me'' – Fe, Co, Cu) compounds decrease at  $R_{Ln^{3+}}$  decreasing (fig. 6), hereby the *c* parameters decreases more strongly than *a* one. Partial substitution of Ba<sup>2+</sup> by other AEE ions in the LaBaFeCuO<sub>5+δ</sub> structure leads to the decreasing of its lattice constants, hereby at substitution degree of Ba<sup>2+</sup> by Sr<sup>2+</sup> on 25 mol. % the formation of new chemical compound LaBa<sub>3/4</sub>Sr<sub>1/4</sub>FeCuO<sub>5+δ</sub> due to ordering of La<sup>3+</sup>, Ba<sup>2+</sup> and Sr<sup>2+</sup> in A site of LaBaFeCuO<sub>5+δ</sub> crystal structure (fig. 7). In the systems YBaFeCoO<sub>5</sub>–YBaFeCuO<sub>5</sub>, YBaFeCoO<sub>5</sub>–YBaCoCuO<sub>5</sub>, YBaFeCuO<sub>5</sub>–YBaCoCuO<sub>5</sub> the continuous regions of the solid solutions are formed,

which lattice constants changed by different ways at substitution of one cation of  $3d$ -metal by other (fig. 8) [65,87].

As can be seen from the fig. 9, the IR absorption spectra of the  $\text{LaBaFeCoO}_{5.97}$  and  $\text{LaBaCoCuO}_{5.62}$  compounds had diffuse character with poorly expressed absorption maxima near  $580 \text{ cm}^{-1}$  ( $\nu_2^*$ ). The IR absorption spectra of the  $\text{LnBaFeCoO}_{5+\delta}$  ( $\text{Ln} = \text{REE}$ ) compounds and  $\text{LaBaFeCuO}_{5.47}$  phase exhibit two distinct bands with maxima at  $368\text{--}372$  ( $\nu_1$ ) and  $582\text{--}604$  ( $\nu_2$ )  $\text{cm}^{-1}$ , and IR absorption spectra of the  $\text{LnBaFeCuO}_{5+\delta}$ ,  $\text{LnBaCoCuO}_{5+\delta}$  ( $\text{Ln} = \text{REE}$ ) oxides and  $\text{PrBaFeCoO}_{5+\delta}$  phase exhibit three distinct bands with maxima at  $360\text{--}384$  ( $\nu_1$ ),  $544\text{--}592$  ( $\nu_2$ ) and  $648\text{--}677$  ( $\nu_3$ )  $\text{cm}^{-1}$  [21,59–61,64,66,69], which are associated with the bending ( $\nu_1$ ) and stretching ( $\nu_2$ ) vibrations of the metal–oxygen bonds in the  $-(\text{Me}',\text{Me}'')\text{O}_2-$  layers and the stretching vibrations ( $\nu_3$ ) of the  $(\text{Me}',\text{Me}'')\text{--O--}(\text{Me}',\text{Me}'')$  bonds containing apical oxygen atoms in the structures of the layered perovskites  $\text{LnBaMe}'\text{Me}''\text{O}_{5+\delta}$  [88].

The facts that band with maximum at  $\nu_3$  was absent on the absorption spectra of the ferrocobaltites and that  $\nu_2 < \nu_2^* < \nu_3$  show that  $3d$ -metal–oxygen ( $3d$ -metal = Fe, Co, Cu) interactions in the  $\text{LnBaFeCoO}_{5+\delta}$  ( $\text{Ln} = \text{REE}$ ) oxides (and in the  $\text{LaBaCuFeO}_{5.47}$  phase) were quasi-isotropic whereas  $3d$ -metal–oxygen distances in the  $-(\text{Fe},\text{Co},\text{Cu})\text{O}_2-$  layers of the  $\text{LnBaCoCuO}_{5+\delta}$  and  $\text{LnBaFeCuO}_{5+\delta}$  ( $\text{Ln} = \text{REE}$ , except La) were larger than in the  $c$  direction (perpendicular to the  $-\text{Fe}(\text{Co},\text{Cu})\text{O}_2$ -layers).

On the fig. 10 present the dependences of the absorption maxima ( $\nu_1, \nu_2, \nu_3$ ) for  $\text{LnBaMe}'\text{Me}''\text{O}_{5+\delta}$  ( $\text{Ln} - \text{REE}$ ;  $\text{Me}', \text{Me}'' - \text{Fe}, \text{Co}, \text{Cu}$ ) layered compound versus lanthanide ionic radii ( $R_{\text{Ln}^{3+}}$ ). As can be seen from the fig. 10, for  $\text{LnBaFeCoO}_{5+\delta}$  phases values  $\nu_1$  and  $\nu_2$  does not depend practically from the  $R_{\text{Ln}^{3+}}$ , but for  $\text{LnBaCoCuO}_{5+\delta}$  and  $\text{LnBaFeCuO}_{5+\delta}$  ones  $\Delta\nu = (\nu_3 - \nu_2)$  values increases at  $R_{\text{Ln}^{3+}}$  increasing for the  $\Theta < 0.25$  region and decreases at  $R_{\text{Ln}^{3+}}$  increasing for the  $\Theta > 0.25$  region. Thus, increasing the  $R_{\text{Ln}^{3+}}$  reduces the metal–oxygen bonds in the  $-(\text{Fe},\text{Co},\text{Cu})\text{O}_2-$  layers and increases in the  $(\text{Me}',\text{Me}'')\text{--O--}(\text{Me}',\text{Me}'')$  chains of the 0112 phases structure (when less than 25% O(3) positions in the 0112 phases structure are occupied). Moreover, with further  $R_{\text{Ln}^{3+}}$  increasing  $\delta$  values also increases (when more than 25% O(3) positions in the 0112 phases structure are occupied) and the metal–oxygen interactions along different crystallographic directions in the crystal structure of  $\text{LnBaCoCuO}_{5+\delta}$  and  $\text{LnBaFeCuO}_{5+\delta}$  phases become less anisotropic.

The lattice constants of the oxygen-deficient  $\text{LnBaMe}'\text{Me}''\text{O}_{5+\delta}$  ( $\text{Ln} - \text{REE}$ ;  $\text{Me}', \text{Me}'' - \text{Fe}, \text{Co}, \text{Cu}$ ) perovskites depend on their oxygen non-stoichiometry and these dependences can be quantitatively characterized using so-called volume chemical expansion coefficient (VCEC), which can be expressed with the equation (8):

$$\alpha_{\delta,V} = -\frac{1}{V_0} \left( \frac{\partial V}{\partial \delta} \right)_T, \quad (8)$$

where  $\alpha_{\delta,V}$  – volume chemical expansion coefficient,

$V_0$  is the unit cell volume at  $\delta = 0.00$  and

$V$  is the unit cell volume at the corresponding value of oxygen non-stoichiometry index ( $\delta$ ).

The sign “minus” in equation (8) is necessary to obtain positive values of the volume CEC ( $\alpha_{\delta,V}$ ) because the unit cell volume increase with a decrease in the  $\delta$  value ( $\left( \frac{\partial V}{\partial \delta} \right) < 0$ ).

The chemical expansion coefficients ( $\alpha_{\delta,V}$ ) some of the layered perovskites  $\text{LnBaMe}'\text{Me}''\text{O}_{5+\delta}$  in different ranges of oxygen non-stoichiometry ( $\delta$ ) are listed in the table 3. It can be seen from table 3 that the chemical expansion coefficients increase with decrease in the oxygen non-stoichiometry (the CEC for the  $\text{LaBaFeCuO}_{5+\delta}$  phase at  $\delta < 0.25$  is four times larger than than at  $0.25 < \delta$ ) and an increase

in the ionic radius of REE (at identical oxygen non-stoichiometry value  $\delta$  the chemical expansion coefficient for the  $\text{LaBaCuFeO}_{5+\delta}$  phase is almost four times larger than that for the  $\text{PrBaCuFeO}_{5+\delta}$  phase). Therefore, the inference can be made that the chemical expansion coefficients for the  $\text{LnBaMe}'\text{Me}''\text{O}_{5+\delta}$  compounds depend on both the ionic radius of lanthanides and the oxygen content in the samples.

Table 3. Volume chemical expansion coefficients ( $\alpha_{\delta,V}$ ) of the  $\text{LnBaFeMeO}_{5+\delta}$  ( $\text{Ln} - \text{La, Pr; Me} - \text{Co, Cu}$ ) phases for different regions of the occupation degree of O(3) positions ( $\Theta$ ) in their crystal structure

Compound	$\alpha_{\delta,V}$	$\Theta$	Ref.
$\text{LaBaFeCoO}_{5+\delta}$	0,057	$0,50 < \Theta < 1,00$	[63]
$\text{LaBaFeCuO}_{5+\delta}$	0,044	$0,00 < \Theta < 0,25$	[89]
	0,011	$0,25 < \Theta < 0,50$	
$\text{PrBaFeCuO}_{5+\delta}$	0,012	$0,00 < \Theta < 0,25$	[89]

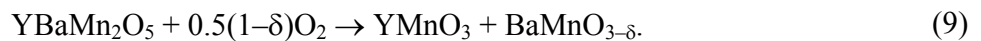
### 3. Thermal stability and thermal expansion

$\text{LnAME}_2\text{O}_{5+\delta}$  ( $\text{Ln} - \text{REE; A} - \text{AE or AEE; Me} - 3d\text{-metal}$ ) compounds at room temperature are thermodynamically stable or can exist for a long time without any changing. When temperature gains they can change their crystal structure (in particular, due to the oxygen vacancies ordering/disordering in their crystal structure) or oxygen content (at heating in air, for example, layered  $\text{LnBaMn}_2\text{O}_5$  manganites are oxidized by atmospheric oxygen but  $\text{LaBaFeCuO}_{5+\delta}$  ferrocuprate is reduced due to loss of oxygen) and, finally, decompose to the complex or binary oxides.

Linear thermal expansion coefficient (LTEC,  $\alpha$ ) of these oxides show a strong anisotropy: they expansivity along  $c$  axis is more pronounced than in basal  $-\text{MeO}_2-$  planes ( $\alpha_c > \alpha_a$ ). The LTEC values of  $\text{LnAME}_2\text{O}_{5+\delta}$  ( $\text{Ln} - \text{REE; A} - \text{AE or AEE; Me} - 3d\text{-metal}$ ) perovskites strongly depend on the nature of REE and oxygen non-stoichiometry value ( $\delta$ ) and change in a wide region (so, depending on the temperature regions and composition the LTEC values of  $\text{LnBaMe}'\text{Me}''\text{O}_{5+\delta}$  phases change within  $(9.6\text{--}30.2) \cdot 10^{-6} \text{ K}^{-1}$  (table 4)).

#### 3.1. $\text{LnBaMe}_2\text{O}_{5+\delta}$ ( $\text{Ln} - \text{Y, REE; Me} - \text{Mn, Fe, Co}$ ) phases

As was mentioned above in this chapter (section 2), the  $\text{YBaMn}_2\text{O}_{5+\delta}$  compound is unstable in air and it can be only prepared in reducing atmospheres [26]. When heated in air or oxygen, this compound decomposes irreversibly into  $\text{YMnO}_3$  and  $\text{BaMnO}_{3-\delta}$  above 493 K [34]:



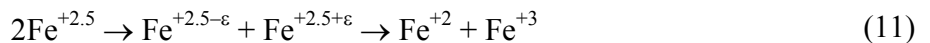
The other manganites described in this chapter are stable in air at high temperatures but change their oxygen content at heating and cooling in air [23,25,40–42]. Annealing of  $\text{LnBaMn}_2\text{O}_{5+\delta}$  manganites at high temperatures can also lead to the disordering of  $\text{Ln}^{3+}$  and  $\text{Ba}^{2+}$  cations on A sites of their perovskite ( $\text{ABO}_3$ ) structure. So, degree of A-site order ( $\varepsilon$ ) for  $\text{PrBaMn}_2\text{O}_6$  ordered manganite ( $\varepsilon = 100\%$ ) at its annealing at 1373, 1473 and 1573 K lowers to the  $\varepsilon = 70, 50$  and  $0\%$  respectively [90]. Such change of cationic distribution in  $\text{PrBaMn}_2\text{O}_6$  structure lead to sharp change in its

properties. The A-site ordered PrBaMn<sub>2</sub>O<sub>6</sub> sample ( $\varepsilon = 100\%$ ) demonstrates ferromagnetic metallic to paramagnetic insulator transition with the Curie point  $\approx 320$  K. The A-site disordered PrBaMn<sub>2</sub>O<sub>6</sub> sample ( $\varepsilon = 0\%$ ) is ferromagnetic metal below  $T_C \approx 140$  K [90].

The  $LnBaFe_2O_{5+\delta}$  ( $Ln - REE$ ) ferrites usually prepared in reducing atmosphere [27,45], but for  $Ln = La, Nd, Sm-Gd$  the  $LnBaFe_2O_{5+\delta}$  phases remain stable in oxygen up to 1273 K [27]. The stability to the oxidative decomposition narrows substantially for smaller  $Ln = Tb-Ho$ , as these phases become stable only in reducing atmospheres. Their oxidation upon gradually increasing partial pressure oxygen proceeds sharply into multiphase products exemplified in equation (10) for  $Ln = Dy$ :



Reductive decomposition of  $LnBaFe_2O_{5+\delta}$  ( $Ln - REE$ ) proceeds at 1273 K at  $\log(p_{O_2}, \text{bar}) \approx -16.6 \div -15.2$  (the stability region narrows at decreasing of lanthanide ionic radius) over an intermediate pseudo-equilibrium range into a dark-green product where iron has oxidation state close to +2. By correcting the redox conditions, the green product can be oxidized back to a single-phase double-cell perovskite [27]. The  $\delta$  values for stable  $LnBaFe_2O_{5+\delta}$  double perovskites vary in regions  $\delta = 0.022 \div 0.646$ ,  $-0.002 \div 0.046$ ,  $0.006 \div 0.045$  and  $0.000 \div 0.031$  for  $Ln = Sm, Tb, Dy$  and  $Ho$  respectively [27,45].  $LnBaFe_2O_{5+\delta}$  ferrites undergo the so-called Verwey transition – charge ordering or the iron cations:



at temperatures  $T_V = 214 \pm 1, 232 \pm 6, 252 \pm 9, 267 \pm 7, 282 \pm 5, 290 \pm 7, 293 \pm 17$  and  $307 \pm 6$  K for  $NdBaFe_2O_5, SmBaFe_2O_5, EuBaFe_2O_5, GdBaFe_2O_5, TbBaFe_2O_5, DyBaFe_2O_5, HoBaFe_2O_5$  and  $YBaFe_2O_5$  respectively. Increasing of oxygen content ( $\delta$ ) in ferrites  $LnBaFe_2O_{5+\delta}$  leads to the lowering of  $T_V$  temperature [27].

Layered  $LnBaCo_2O_{5+\delta}$  ( $Ln - REE$ ) cobaltites reversibly exchange by weakly-bound oxygen ( $\delta$ ) with environment at temperatures within 670–1490 K in air [49]. Among the samples described in this subsection, layered cobaltites are the most stable compounds.

### 3.2. $LnBaMe'Me''O_{5+\delta}$ ( $Ln - Y, REE; Me', Me'' - Fe, Co, Cu$ ) phases

The  $LnBaMe'Me''O_{5+\delta}$  ( $Ln - Y, REE; Me', Me'' - Fe, Co, Cu$ ) compounds are thermally stable in air up to temperature about 673 K. At  $T > 673$  K the reversible exchange by weakly-bound oxygen ( $\delta$ ) between these phases and environment take place [60,61,63] like the layered  $LnBaCo_2O_{5+\delta}$  phases. The temperature when oxygen loss begins decreases at decreasing of partial pressure of oxygen [91]. Partial substitution of Ba by other AEE in  $LaBaFeCuO_{5+\delta}$  leads to decreasing of temperature when oxygen loss begins. These temperatures for  $LaBa_{0.75}Me_{0.25}FeCuO_{5+\delta}$  solid solutions consist 520, 470 and 650 K for  $Me = Sr, Ca$  and  $Mg$  respectively [86]. According to the results of coulometric titration of  $LaBaFeCuO_{5+\delta}$  (fig. 11), the oxygen exchange between sample and environment during heating and cooling proceeds in two stages. This fact depict that weakly-bound oxygen exists in the structure of layered  $LaBaFeCuO_{5+\delta}$  ferrocuprate in two forms which differ energetically, hereby this labile oxygen divides by equal parts between these forms.

Typical dilatometric curves (temperature dependences of the relative elongation ( $\Delta l/l_0$ ) and linear thermal expansion coefficient (LTEC,  $\alpha$ )) for  $LnBaMe'Me''O_{5+\delta}$  ( $Ln - Y, REE; Me', Me'' - Fe, Co, Cu$ ) perovskites are given on the fig. 12. The dependence  $\Delta l/l_0 = f(T)$  is characterized by an anomaly in the form of inflection at temperature about 650 K (for  $LnBaMe'Me''O_{5+\delta}$  phases this temperature varies within 465–820 K (see table 4)), which is accompanied by an increase in the LTEC value. According to the results obtained from the thermogravimetric analysis [60], the release of the weakly-bound oxygen

( $\delta$ ) from the samples begins to occur at temperatures close to 670 K. So, obtained increasing of LTEC values is bound only with chemical expansion of the samples due to increasing of oxygen vacancies concentration in their structure.

The LTEC values for the  $LnBaMe'Me''O_{5+\delta}$  oxides, as a rule, slightly depend on the nature of  $3d$ -metal and decrease at decreasing of ionic radius of lanthanide ion in their composition (table 4). Note that maximal values of LTEC  $LnBaMe'Me''O_{5+\delta}$  compounds in high-temperature regions are found for the samples with maximal content of labile oxygen ( $\delta$ ).

Table 4. Values of linear thermal expansion coefficient ( $\alpha$ ) of the  $LnBaMe'Me''O_{5+\delta}$  ( $Ln - Y, REE; Me', Me'' - Fe, Co, Cu$ ) for different temperature regions

Compound	$10^6 \cdot \alpha, K^{-1}$	$T, K$	Ref.
1	2	3	4
YBaMnCoO <sub>5.004</sub>	9,6(2) ( $\alpha_a$ ), 18,2(4) ( $\alpha_c$ )	200–300	[58]
YBaFeCoO <sub>5+\delta</sub>	12,2	300–520	[59]
	17,3	520–1100	
YBaCoCuO <sub>5+\delta</sub>	14,3	300–1100	[66]
YBaCoCuO <sub>5+\delta</sub>	14,7	300–1100	[87]
YBaFeCuO <sub>5+\delta</sub>	12,3	300–1100	[60]
LaBaFeCoO <sub>5+\delta</sub>	13,5	300–770	[63]
	30,2	770–1100	
LaBaCoCuO <sub>5+\delta</sub>	12,6	300–530	[63]
	20,3	530–1100	
LaBaFeCuO <sub>5+\delta</sub>	14,4	300–600	[60]
	20,2	650–1100	
PrBaFeCoO <sub>5+\delta</sub>	16,8	300–820	[64]
	25,4	820–1100	
PrBaCoCuO <sub>5+\delta</sub>	14,6	300–705	[64]
	19,0	705–1100	
PrBaFeCuO <sub>5+\delta</sub>	15,3	300–1100	[60]
NdBaCoCuO <sub>5+\delta</sub>	12,5	300–575	[61]
	18,8	575–1100	
NdBaFeCuO <sub>5+\delta</sub>	14,8	300–1100	[60]
SmBaCoCuO <sub>5+\delta</sub>	12,0	300–575	[61]
	16,1	575–1100	
SmBaFeCuO <sub>5+\delta</sub>	15,5	300–1100	[60]
EuBaFeCuO <sub>5+\delta</sub>	14,7	300–1100	[60]
GdBaCoCuO <sub>5+\delta</sub>	9,60	300–500	[61]
	14,9	500–1100	
GdBaFeCuO <sub>5+\delta</sub>	13,3	300–1100	[60]
TbBaFeCoO <sub>5+\delta</sub>	11,5	300–500	[59]
	19,3	500–1100	
TbBaFeCuO <sub>5+\delta</sub>	13,8	300–1100	[60]
DyBaFeCoO <sub>5+\delta</sub>	11,8	300–465	[59]
	18,4	465–1100	
DyBaCoCuO <sub>5+\delta</sub>	14,7	300–1100	[66]
DyBaFeCuO <sub>5+\delta</sub>	13,3	300–1100	[60]
HoBaFeCoO <sub>5+\delta</sub>	12,3	300–535	[59]
	17,9	535–1100	
HoBaCoCuO <sub>5+\delta</sub>	15,1	300–1100	[69]
HoBaFeCuO <sub>5+\delta</sub>	13,1	300–1100	[60]
ErBaFeCuO <sub>5+\delta</sub>	12,7	300–1100	[60]
TmBaFeCuO <sub>5+\delta</sub>	13,5	300–1100	[60]

1	2	3	4
YbBaFeCuO <sub>5+δ</sub>	14,6	300–1100	[60]
LuBaFeCuO <sub>5+δ</sub>	12,8	300–1100	[60]

The  $LnBaMe'Me''O_{5+\delta}$  compounds show the strong anisotropy in LTEC values. As it was found in [58,92] the thermal expansivity of the samples along  $c$  axis (perpendicular to  $-(Me'.Me'')O_2-$  planes) ( $\alpha_c$ ) up to two times larger than in the  $-(Me'.Me'')O_2-$  planes ( $\alpha_a$ ).

As it was mentioned above, expansion of the 0112 layered perovskites at high temperatures exhibits both the thermal (an enhancement of the anharmonicity of vibrations) and chemical (an increase in the number of oxygen vacancies) nature. The separation of thermal and chemical expansions for oxygen-non-stoichiometric oxides is a topical problem.

The separation of the thermal (linear thermal expansion coefficient ( $\alpha_T$ ) and chemical (linear chemical expansion coefficient ( $\alpha_\delta$ ) contributions to the linear expansion of the samples can be carried out using equations (12,13) for the dilatometric results [61,63]:

$$\alpha_T = \frac{1}{l_0} \left( \frac{\partial \Delta l}{\partial T} \right)_\delta, \quad (12)$$

$$\alpha_\delta = \frac{1}{l_0} \left( \frac{\partial \Delta l}{\partial \delta} \right)_T, \quad (13)$$

and equation (14–16) for the results of high-temperature XRD [92]:

$$a_{T,\delta} = a_{T_0,\delta_0} \cdot [1 + \alpha_T \cdot (T - T_0) + \alpha_\delta \cdot (\delta - \delta_0)], \quad (14)$$

$$\alpha_T = \frac{1}{a_{T_0,\delta_0}} \left( \frac{\partial a}{\partial T} \right)_{P,\delta}, \quad (15)$$

$$\alpha_\delta = -\frac{1}{a_{T_0,\delta_0}} \left( \frac{\partial a}{\partial \delta} \right)_{T,P}, \quad (16)$$

where  $a_{T,\delta}$  - value of lattice constant of perovskite at some values of temperature ( $T$ ) and oxygen non-stoichiometry ( $\delta$ ) of the sample;  $a_{T_0,\delta_0}$  - value of lattice constant of the sample at initial values of temperature ( $T_0$ ) and oxygen non-stoichiometry ( $\delta_0$ ) of the sample.

Fig. 13 illustrates the separation of the thermal expansiveness ( $\alpha_T$ ) and the chemical expansiveness ( $\alpha_\delta$ ) from the  $a = f(T)$  function and the unit-cell jump due to the disorder of the oxygen lattice, ( $\Delta a$ ), for LaBaCuFeO<sub>5+δ</sub> phase.

At calculations of  $\alpha_T$  and  $\alpha_\delta$  in [61,63,92] it had been assumed that, to a first approximation, the degree of anharmonicity of the vibrations was determined only by the temperature and did not depend on the number of oxygen vacancies in the crystal structure of the layered  $LnBaMe'Me''O_{5+\delta}$  perovskites. The linear thermal expansion coefficients ( $\alpha_T$ ) and the linear chemical expansion coefficients ( $\alpha_\delta$ ) of the  $LnBaMe'Me''O_{5+\delta}$  phases are presented in the table 5. As can be seen from these data, the thermal expansivity of the samples studied takes over the close values but the chemical expansiveness of ferrocobaltites ( $LnBaFeCoO_{5+\delta}$  phases) and cuprocobaltites ( $LnBaCoCuO_{5+\delta}$  phases) large than chemical expansiveness of ferrocuprates ( $LnBaFeCuO_{5+\delta}$  phases), probably, due to the more lower oxygen content in the latters.

Table 5. Values of linear thermal ( $\alpha_T$ ) and chemical ( $\alpha_\delta$ ) expansion coefficient of the  $LnBaMe'Me''O_{5+\delta}$  ( $Ln - La, Pr, Nd$ ;  $Me', Me'' - Fe, Co, Cu$ ) layered perovskites

Compound	$10^6 \cdot \alpha_T, K^{-1}$	$10^3 \cdot \alpha_\delta$	Ref.
LaBaFeCoO <sub>5+δ</sub>	13,2	17,3	[63]
LaBaCoCuO <sub>5+δ</sub>	11,5	15,7	[63]
NdBaCoCuO <sub>5+δ</sub>	12,5	16,3	[61]
LaBaFeCuO <sub>5+δ</sub>	12,4	9,20	[92]
PrBaFeCuO <sub>5+δ</sub>	12,2	8,72	[92]
LaBa <sub>0,5</sub> Sr <sub>0,5</sub> FeCuO <sub>5+δ</sub>	11,7	7,55	[92]

#### 4. Magnetic properties

The  $LnAMe'Me''O_{5+\delta}$  ( $Ln - REE$ ;  $A - AE, AEE$ ;  $Me'', Me'' - 3d$ -metal) oxides demonstrate of richness of magnetic properties due to different types of ordering of magnetic ions in their crystal structure. They are ferromagnetic (FM) and anti-ferromagnetic (AFM), which Curie and Neel temperatures range in a wide limits depending on the nature of cations in the structure of  $LnBaMe'Me''O_{5+\delta}$  phases and their oxygen non-stoichiometry values. Some of  $LnBaMe'Me''O_{5+\delta}$  demonstrate colossal magneto-resistance.

##### 4.1. $LnBaMe_2O_{5+\delta}$ ( $Ln - Y, REE$ ; $Me - Mn, Fe, Co$ ) phases

LaAMn<sub>2</sub>O<sub>5+δ</sub> ( $A - K, Rb$ ) phases are ferromagnetic with Curie temperatures ( $T_C$ ) of  $327 \pm 1$  and  $290 \pm 3$  K for  $A = K$  and  $Rb$  respectively [23]. The experimentally measured values of saturation magnetization,  $M_S$ , are equal to  $74 \pm 2$  and  $64 \pm 2$  emu·g<sup>-1</sup> respectively. These values are smaller than the corresponding values, 104.6 and 91.1 emu·g<sup>-1</sup>, calculated using the formula (17):

$$M_S = g\mu_B \langle S \rangle, \quad (17)$$

where  $g = 2$  is Lande  $g$  factor,  $\mu_B$  is the Bohr magneton, and  $\langle S \rangle$  is the average spin value, for the appropriate Mn(III) and Mn(IV) content. The discrepancy could in part be due to the presence of alkali cations which render the sample sensitive to atmospheric CO<sub>2</sub> and H<sub>2</sub>O. Another possibility is that these oxides possess a canted ferromagnetic structure. Although LaCsMn<sub>2</sub>O<sub>5,59</sub> exhibits the onset of the spontaneous magnetization around 170 K, the transition is very broad, and zero-field-cooled temperature dependence of the magnetization is similar to the spin glass behavior. So, LaCsMn<sub>2</sub>O<sub>5,59</sub> phase most probably does not have a long-range ferromagnetic order at low temperature [23]. Measurement of magneto-resistance at an applied field of  $H = 5$  T shows a clear suppression of resistivity (up to about -40% and -30% for  $A = K$  and  $Rb$  respectively) indicating the presence of colossal magneto-resistance (CMR) effect in the LaAMn<sub>2</sub>O<sub>5+δ</sub> ( $A - K, Rb$ ) phases. Presence of considerable magneto-resistance (MR) at low temperature can be attributed to the grain boundary effects in ceramic samples.

YBaMn<sub>2</sub>O<sub>6</sub> compound show a number of magnetic phase transitions [13,38] (table 6). At high temperatures above  $T_{C,1} = 520$  K the  $\chi = f(T)$  curve shows a paramagnetic behavior obeying the Curie-Weiss law with the effective moment  $P_{\text{eff}} = 8.06 \mu_B$  and Weiss constant  $\Theta_1 = 286$  K. The positive value of  $\Theta_1$  suggests the ferromagnetic spin correlation and the value of  $P_{\text{eff}}$  is compatible with a theoretical value of  $7.94 \mu_B$  derived from  $[Mn^{3+} + Mn^{4+}]$  in YBaMn<sub>2</sub>O<sub>6</sub>. Upon decreasing temperature  $\chi$  drops sharply at  $T_{C,1}$  while only small anomaly is observed at  $T_{C,2}$  where metal-insulator (IM) transition occurs. Below  $T_{C,2}$  the  $\chi = f(T)$  curve once again shows a paramagnetic behavior but the Curie-Weiss

fitting gave a negative value of  $\Theta_2 = -379$  K, indicating an anti-ferromagnetic interaction. Finally,  $\chi$  exhibits a steep drop at  $T_{C,3}$  then reaching a constant value  $\approx 0.006$  emu·(mol Mn)<sup>-1</sup>. Considering the negative value of  $\Theta_2$ , it is natural to assume that the transition at  $T_{C,3}$  would be due to the anti-ferromagnetic long-range order [38].

Table 6. Temperatures of magnetic phase transitions of  $LnAMe_2O_{5+\delta}$  ( $Ln$ – Y, A – AE, Ba; REE; Me – Mn, Co) oxides

Compound	$T$ , K	Transition type	Ref.
1	2	3	4
LaKMn <sub>2</sub> O <sub>5,53</sub>	327	FM (ferromagnetic) → PM (paramagnetic)	[23]
LaRbMn <sub>2</sub> O <sub>5,53</sub>	290	FM → PM	[23]
LaCsMn <sub>2</sub> O <sub>5,6</sub>	170	SG (spin glass) → PM	[23]
YBaMn <sub>2</sub> O <sub>6</sub>	200	AFMI (anti-ferromagnetic insulator) → PMI (paramagnetic insulator)	[13,38]
	480	PMI → PMM <sub>2</sub> (paramagnetic metal)	
	520	PMM <sub>2</sub> → PMM <sub>1</sub>	
YBaMn <sub>2</sub> O <sub>5+δ</sub>	166	AFM (anti-ferromagnetic) → PM	[35]
YBaMn <sub>2</sub> O <sub>5</sub>	165	AFM [G type] → PM	[36]
LaBaMn <sub>2</sub> O <sub>5,5</sub>	185	AFM → PM	[40]
PrBaMn <sub>2</sub> O <sub>6</sub>	320	FM → PM	[25,90]
NdBaMn <sub>2</sub> O <sub>6</sub>	310	FM → PM	[25]
SmBaMn <sub>2</sub> O <sub>6</sub>	280	FM → PM	[25]
EuBaMn <sub>2</sub> O <sub>6</sub>	260	FM → PM	[25]
GdBaMn <sub>2</sub> O <sub>6</sub>	250	FM → PM	[25]
TbBaMn <sub>2</sub> O <sub>6</sub>	160	FM → PM	[25]
YBaCo <sub>2</sub> O <sub>5+δ</sub>	≈185 (≈260)*	AFM → FM	[48]
	259 (293)*	FM → PM	
YBaCo <sub>2</sub> O <sub>5,44</sub>	190	AFM → wFM (weak ferromagnetic)	[47]
	260	wFM → PM	
YBaCo <sub>2</sub> O <sub>6</sub>	250	FM → PM	[94]
LaBaCo <sub>2</sub> O <sub>6</sub>	225	FM → PM	[94]
LaBaCo <sub>2</sub> O <sub>5+δ</sub>	179,16	FM → PM	[28]
PrBaCo <sub>2</sub> O <sub>6</sub>	150	FM → PM	[94]
PrBaCo <sub>2</sub> O <sub>5+δ</sub>	76,5	AFM → FM	[28]
	115,71	FM → PM	
NdBaCo <sub>2</sub> O <sub>6</sub>	140,260	FM → PM	[94]
NdBaCo <sub>2</sub> O <sub>5+δ</sub>	107,9	AFM → FM	[28]
	246,7	FM → PM	
SmBaCo <sub>2</sub> O <sub>6</sub>	120–200	AFM → FM	[94]
	280	FM → PM	
SmBaCo <sub>2</sub> O <sub>5+δ</sub>	221,7	AFM → FM	[28]
	263,9	FM → PM	
EuBaCo <sub>2</sub> O <sub>6</sub>	150–240	AFM → FM	[94]
	280	FM → PM	
EuBaCo <sub>2</sub> O <sub>5+δ</sub>	236,5	AFM → FM	[28]
	282,9	FM → PM	
GdBaCo <sub>2</sub> O <sub>6</sub>	225	AFM → FM	[93]
	280	FM → PM	
GdBaCo <sub>2</sub> O <sub>6</sub>	220	AFM → FM	[54]
	285	FM → PM	
GdBaCo <sub>2</sub> O <sub>5+δ</sub>	242,9	AFM → FM	[28]
	278,3	FM → PM	
GdBaCo <sub>2</sub> O <sub>6</sub>	250	AFM → FM	[94]

1	2	3	4
TbBaCo <sub>2</sub> O <sub>6</sub>	245	AFM → FM	[94]
	285	FM → PM	
TbBaCo <sub>2</sub> O <sub>5+δ</sub>	254,1	AFM → FM	[28]
	282,4	FM → PM	
DyBaCo <sub>2</sub> O <sub>6</sub>	265	FM → PM	[94]
DyBaCo <sub>2</sub> O <sub>5,5</sub>	300	FM → PM	[96]
DyBaCo <sub>2</sub> O <sub>5+δ</sub>	188,6	AFM → FM	[28]
	260,6	FM → PM	
HoBaCo <sub>2</sub> O <sub>5+δ</sub>	178,2	AFM → FM	[27]
	286,2	FM → PM	

\*Data for sample slowly cooled (quenched) in air from 1273 K.

In [36] for YBaMn<sub>2</sub>O<sub>5</sub> the magnetic transition at 165 K had been observed and a ferromagnetic component had been clearly revealed by the peak in the imaginary part of alternate current (AC) susceptibility. However, the saturated moment from direct current (DC) measurement at 5 K was only 0.95  $\mu_B$  per YBaMn<sub>2</sub>O<sub>5</sub> formula unit, which could be compared with the total moment of 9  $\mu_B$  per YBaMn<sub>2</sub>O<sub>5</sub> that would result from a ferromagnetically ordered array of  $S = 5/2$  Mn<sup>2+</sup> and  $S = 2$  Mn<sup>3+</sup> spins. The neutron diffraction data results showed that the order is ferromagnetic. If all of the  $S = 5/2$  Mn<sup>2+</sup> spins were anti-parallel to the  $S = 2$  Mn<sup>3+</sup> spins, a saturated moment of 1  $\mu_B$  per YBaMn<sub>2</sub>O<sub>5</sub> formula unit was expected. This was consistent with the observed value of 0.95  $\mu_B$  [36].

According to the magnetic susceptibility measurements, in the LaBaMn<sub>2</sub>O<sub>5,5</sub> manganite the anti-ferromagnetic ordering of Mn<sup>3+</sup> cations at  $T_N = 185$  K take place [40]. The other ordered  $Ln$ BaMn<sub>2</sub>O<sub>6</sub> ( $Ln = \text{Pr, Nd, Sm, Eu, Gd, Tb}$ ) phases are ferromagnetic at low temperatures [25] and their Curie temperature ( $T_C$ ) decreases at decreasing of lanthanide ionic radii (table 6).

In [47] the temperature dependence of magnetization of YBaCo<sub>2</sub>O<sub>5,44</sub> oxide had been measured. The magnetization sharply increased below 260 K and then suddenly decreased below 190 K. The  $M$ - $H$  curves indicated a paramagnetic (PM) to weak-ferromagnetic (wFM) transition at 260 K and a wFM to anti-ferromagnetic (AFM) transition at 190 K. The magnetic moment estimated from  $M$ - $H$  curves was about 0.30  $\mu_B/\text{Co}$  in the wFM state for sample studied. The magnetization in field cooling (FC) measurements was slightly different from that in zero field cooling (ZFC) measurements, and it showed a cluster-glass-like behavior below 80 K [47].

The magnetization ( $M$ ) measurements for  $Ln$ BaCo<sub>2</sub>O<sub>5+δ</sub> series had been performed in [28]. The  $M = f(T)$  dependence for LaBaCo<sub>2</sub>O<sub>5+δ</sub> ( $Ln = \text{La, Pr, Nd, Sm, Eu, Gd, Tb, Dy, Ho}$ ) was typical for ferromagnetic ordering with  $T_C = 179$  K. The compounds with light rare earths ( $Ln = \text{Pr-Eu}$ ) showed basically similar  $M = f(T)$  behavior. With a decrease in temperature, PrBaCo<sub>2</sub>O<sub>5+δ</sub> made a PM to FM transition with  $T_C = 115$  K. The sharp decrease of magnetization below  $T_C$  indicated the likelihood of the presence of anti-ferromagnetic interactions in this compound. For NdBaCo<sub>2</sub>O<sub>5+δ</sub> two transitions had been observed at 107 and 246 K, respectively. Authors attributed the transition at 246 as due to cobalt ions but the origin the transition at 107 K was not clear. The  $Ln$ BaCo<sub>2</sub>O<sub>5+δ</sub> ( $Ln = \text{Sm, Eu}$ ) compounds pass through several magnetic states within 5–400 K. Near 250 K, the magnetization increased steeply and the compounds went from AFM to FM state followed by a FM to PM transition. For the heavy rare-earth-based  $Ln$ BaCo<sub>2</sub>O<sub>5+δ</sub> ( $Ln = \text{Gd-Ho}$ ) compounds, the temperature dependent magnetization showed paramagnetic behavior in the low-temperature region and weak ferromagnetism in the temperature range 190–260 K, with an anti-ferromagnetic phase in between. The effective paramagnetic moments was calculated as 8.52  $\mu_B/\text{f.u.}$  (formula unit), 9.98  $\mu_B/\text{f.u.}$ , 10.34  $\mu_B/\text{f.u.}$  and 10.66  $\mu_B/\text{f.u.}$  for  $Ln = \text{Gd, Tb, Dy and Ho}$ , respectively. Since these values were very near to the  $p_{\text{eff}}$

value the free  $Ln^{3+}$  ion, it implied that at least for the heavy rare-earth-based  $LnBaCo_2O_{5+\delta}$  system, Co had no negligibly small moment in the low-temperature region [28].

#### 4.2. $LnBaMe'Me''O_{5+\delta}$ ( $Ln - Y, REE; Me', Me'' - Fe, Co, Cu$ ) phases

All the described in this chapter  $LnBaMe'Me''O_{5+\delta}$  ( $Ln - Y, REE; Me', Me'' - Fe, Co, Cu$ ) compounds are anti-ferromagnetics at low temperatures (table 7), excluding  $LaBaFeCoO_{5+\delta}$  phase in which the ferromagnetic ordering below 168 K occurs [63].

Table 7. Temperature of magnetic phase transitions of  $LnMMe'Me''O_{5+\delta}$  ( $Ln - Y, REE; M - AEE; Me', Me'' - Mn, Fe, Co, Cu$ ) layered perovskites

Compound	$T, K$	Transition type	Ref.
YBaMnCoO <sub>5</sub>	190	AFM → PM	[58]
YBaFeCuO <sub>5+δ</sub>	446	AFM → PM	[70]
LaBaFeCoO <sub>5+δ</sub>	168	FM → PM	[63]
YSrFeCuO <sub>5+δ</sub>	400	AFM → PM	[77]
YBaFeCuO <sub>5+δ</sub>	460	AFM → PM	[12]
YBaFeCuO <sub>5+δ</sub>	240	AFM <sub>2</sub> → AFM <sub>1</sub>	[72]
	475	AFM <sub>1</sub> → PM	
YBaFeCuO <sub>5+δ</sub>	190	AFM <sub>2</sub> → AFM <sub>1</sub>	[97]
	442	AFM <sub>1</sub> → PM	
YBaFeCuO <sub>5+δ</sub>	200	AFM <sub>2</sub> → AFM <sub>1</sub>	[98]
	450	AFM <sub>1</sub> → PM	
YBaFeCuO <sub>5+δ</sub>	442,4(5)	AFM → PM	[73]
LaBaFeCuO <sub>5+δ</sub>	68(3)	AFM → PM	[80]
PrBaFeCuO <sub>5</sub>	380(5)	AFM → PM	[81]
LuBaFeCuO <sub>5+δ</sub>	303(3)	AFM → PM	[82,83]
YBaCoCuO <sub>5</sub>	536	AFM → PM	[62]
YBaCoCuO <sub>5</sub>	422	AFM → PM	[93]
LaBaCoCuO <sub>5+δ</sub>	205	AFM → PM	[68]

The value of Neel temperature for these oxides vary within 68 K (for  $LaBaFeCuO_{5+\delta}$  [80]) to 536 K (for  $YBaCoCuO_5$  [62]) (table 7). For  $YBaFeCuO_5$  phase two magnetic phase transitions had been found [72,97,98]. A first anti-ferromagnetic transition was observed at  $T_{N,1} \approx 475$  K and a second well-defined transition was found at  $T_{N,2} \approx 240$  K. At low temperatures ( $T \approx 20$  K) a third anomaly was observed. According to the neutron powder diffraction study [72,97], the transition at  $T_{N,1}$  is paramagnetic to anti-ferromagnetic phase transition but at  $T_{N,2}$  the commensurate AFM – incommensurate AFM phase transition occurs.

Substitution of Co by Cu in  $YBaCo_{2-x}Cu_xO_5$  solid solutions leads to the increasing of their Neel temperature ( $T_N$ ), hereby the  $T_N = f(x)$  dependence has a complex character (fig. 14) due to changes in the charge and spin state of cobalt ions in these compounds.

### 5. Electric properties

The  $LnBaMe'Me''O_{5+\delta}$  ( $Ln - REE; Me', Me'' - 3d$ -metals) compounds, as a rule, are the  $p$ -type semiconductors, which electrical conductivity values change in a wide range, from  $8 \cdot 10^{-6} \text{ S} \cdot \text{m}^{-1}$  to  $5 \cdot 10^4 \text{ S} \cdot \text{m}^{-1}$  at room temperature, though depending on composition and temperature, some  $LnBaMe'Me''O_{5+\delta}$  demonstrate metallic character of conductivity and major charge carriers in these

phases are the electrons. Layered  $LnBaMe_2O_{5+\delta}$  ( $Ln$  – REE;  $Me$  – Mn, Co) show the insulator (semiconductor) – metal phase transition,  $LnBaFe_2O_{5+\delta}$  oxides also possess the Verwey transition. Some of the  $LnBaCo_2O_{5+\delta}$  and  $LnBaFeCuO_{5+\delta}$  compounds demonstrate large values of thermo-e.m.f. and can be used as oxide thermoelectric.

### 5.1. $LnBaMe_2O_{5+\delta}$ ( $Ln$ – Y, REE; $Me$ – Mn, Fe, Co) phases

Electrical conductivity of  $YBaMn_2O_6$  consist about  $10^{-4} S \cdot m^{-1}$  around 100 K, increases at temperature increasing, has two small anomalies at 200 K (where AFM–PM phase transition take place) and 520 K (where  $PM_1$ – $PM_2$  phase transition occurs) and sharply increases at 480 K where insulator (I) to metal (M) phase transition take place [13,38]. Above 480 K the conductivity value is about  $10^3 S \cdot m^{-1}$  and does not change at temperature increasing [38].

The disordered  $PrBaMn_2O_6$  manganite near 100 K has conductivity about  $10 S \cdot m^{-1}$  and demonstrates MI transition at  $\approx 130$  K (table 8) and peak of magneto-resistivity reaching  $\approx 50\%$  in the field of 9 kOe. The value of conductivity at low temperatures (in so-called metallic state) is considerably lower than Mott's value of minimal metallic conductivity. The peak of magneto-resistivity slightly below its Curie temperature ( $T_C = 140$  K) is very typical for the hole-doped manganites. For the ordered  $PrBaMn_2O_6$  sample the conductivity is about  $10^3 S \cdot m^{-1}$  around 100 K and in the magnetically ordered state starts to increase as temperature decreases. The temperature corresponding to the minimal conductivity value is slightly below the Curie point  $\approx 320$  K. Near the  $T_C$  there is a maximum of magneto-resistance ( $\approx 10\%$ ) observed as in the case of classic magnetic semiconductors. The gradual magneto-resistance increase has been observed as temperature decreased that is characteristic of conducting magnetic ceramics. This type of magneto-resistance is due to an inter-granular electrical transport [90].

Table 8. Temperatures of electrical phase transitions of  $LnBaMe_2O_{5+\delta}$  ( $Ln$ – Y, REE;  $Me$  – Mn, Fe, Co) oxides

Compound	$T$ , K	Transition type	Ref
$YBaMn_2O_6$	480	IM (insulator to metal)	[13,38]
$PrBaMn_2O_6$ (disordered)	130	IM	[90]
$PrBaMn_2O_6$ (ordered)	320	IM	[90]
$YBaCo_2O_{5+\delta}$	294	IM	[48]
$PrBaCo_2O_{5.48}$	344	IM	[14]
$NdBaCo_2O_6$	360	SM (semiconductor to metal)	[94]
$NdBaCo_2O_{5.5}$	360	MI	[101]
$SmBaCo_2O_6$	370	SM	[94]
$EuBaCo_2O_6$	350	SM	[94]
$GdBaCo_2O_6$	360	SM	[94]
$GdBaCo_2O_{5.5}$	370	IM	[95]
$GdBaCo_2O_{5.5}$	360	MI	[101]
$TbBaCo_2O_6$	337	SM	[94]
$TbBaCo_2O_{5+\delta}$	340	IM	[55]
$DyBaCo_2O_6$	330	SM	[94]
$DyBaCo_2O_{5.5}$	320	IM	[96]

The electrical resistivity of  $SmBaFe_2O_{5+\delta}$  had semiconducting character and fell at Verwey temperature ( $T_V = 216$  and  $234$  K for  $\delta = 0.0$  and  $0.1$  respectively). At  $T_V$  there was a change in the activation energy,  $E_A$ , which results in a strong increase in the slope of the  $\rho = f(T)$  curves. An estimate of the activation energy was made using the equation (18):

$$\rho = \rho_0 \exp(E_A / k_B T), \quad (18)$$

where  $\rho_0$  was a constant and  $k_B$  Boltzmann's constant. In the temperature region above  $T_V$  the plot  $\ln\rho = f(1/T)$  appeared to be linear as expected for semiconductors. The slopes corresponded to activation energies of 0.18 and 0.33 eV for samples with  $\delta = 0.1$  and 0.0 respectively. Below  $T_V$  the dependence  $\ln\rho = f(1/T)$  deviated from a linear one, but at least for the sample with  $\delta = 0.1$  the activation energy was higher than above the transition temperature. The deviation from a linear dependence at  $T < T_V$  may suggest that the charge carriers propagate by a hopping mechanism. Additionally a hysteresis behavior in the region around the transition temperature was observed, which could be related to a frustration effect caused by the charge separation [99].

In [100] had been found that below  $T_V$  electrical transport of  $\text{GdBaFe}_2\text{O}_{5+\delta}$  approached a variable-range hopping mechanism, given that a reasonable linearity against  $T^{-1/4}$  was observed towards the lowest temperature limits. Such behavior is often observed for localized electron states. In the fully valence-mixed range (above  $T_V$ ), an Arrhenius-type activation gave a reasonable linear fit, which further slightly implied with the application of diffusion-assisted hopping model (19):

$$\sigma = \left( \frac{eN_c}{a_{sp}^3} \right) \mu \exp\left( -\frac{E_\mu}{k_B T} \right), \quad (19)$$

where the mobility  $\mu$  was given by (20):

$$\mu = eh_p a_{sp}^2 \frac{\nu}{k_B T}. \quad (20)$$

In equations (19) and (20)  $h_p$  was the hopping probability,  $N_c$  the number of carriers per single-perovskite cell,  $a_{sp}$ ,  $a_{sp}$  the average edge of such a cell,  $e$  the electron charge,  $k_B$  the Boltzmann constant,  $E_\mu$  the activation energy, and  $\nu$  the hopping frequency. Assuming that the hopping occurred between neighboring iron sites,  $a_{sp}$  was approximated as the edge of the average single-perovskite cubic unit cell of the phase, calculated from the room-temperature unit-cell parameters. Assuming further that the hopping probability was  $h_p = 1/5$  (instead of the usual  $1/6$  for the octahedral site),  $E_\mu$  and  $\nu N_c$  were extracted as two parameters of least-squares fitting to the experimental data.

Energy  $E_\mu$  had a minimum for compositions about  $\delta = 0.12$  that corresponded to the maximum in conductivity. Around this level of oxygen non-stoichiometry, the concentration of the valence-mixed state is still high enough to make a significant contribution to conductivity, while the ratio between the formally di- and tri-valent iron becomes increasingly favorable for percolations of the valence-mixed  $\text{Fe}^{2.5+}$  pairs via random fluctuations between alternative neighbors  $\text{Fe}^{2+}$  and  $\text{Fe}^{3+}$ . In fact, this maximum in conductivity (and minimum in activation energy) corresponded to the maximum in product of the concentration of the valence-mixed state and the amount of available choices of di- and tri-valent iron pairs as a function of  $\delta$  [100].

Authors [14] had measured the electrical properties of  $\text{PrBaCo}_2\text{O}_{5+\delta}$  and found that this compound demonstrated a MI transition for  $\delta = 0.48$  at  $T_{MI} = 344$  K. Above  $T_{MI}$  the conductivity of  $\text{PrBaCo}_2\text{O}_{5+\delta}$  provided with polaronic (hole) hopping mechanism with  $E_A \approx 0.04$  eV. It was also found that oxygen vacancy disorder above  $T_{OD} = 776$  K reduced hole conductivity, due to the loss of an ideal alternation of  $\text{CoO}_5$  pyramidal and  $\text{CoO}_6$  octahedral planes along the  $b$  direction. The thermo-e.m.f. of  $\text{PrBaCo}_2\text{O}_{5+\delta}$  was very low ( $0 < S < 1 \mu\text{V}\cdot\text{K}^{-1}$ ), increased at temperature increasing and remained almost constant above  $T_{OD}$  [14].

The resistivity of the  $\text{LnBaCo}_2\text{O}_{5+\delta}$  ( $\text{Ln} = \text{Nd}, \text{Gd}$ ) compounds at low temperatures had semiconducting character and was enough large (for  $\delta = 0.165$  at  $T = 100$  K the  $\rho$  values were about

$10^2 \Omega \cdot \text{m}$  for both phases) and values of  $\rho$  as well as the course of  $\rho = f(T)$  dependences strongly depended on the oxygen content. For oxygen concentrations close to the parent composition  $\delta = 0.5$ ,  $\rho = f(T)$  curves showed a sharp metal-insulator(MI) transition upon cooling below approximately the same temperature  $T_{MI} = 360 \text{ K}$ , while the MI transition seems to be smeared for  $\delta$  away from 0.5. Nevertheless, the low-temperature resistivity exhibited a hopping character for the entire range  $0 < \delta < 0.7$ , which allowed authors of [101] us to consider the charge transport in terms of hopping of localized electrons( $\text{Co}^{2+}$ ) or holes ( $\text{Co}^{4+}$ ). In the insulating regime, the resistivity in both compounds quickly decreased with hole doping ( $\delta$  increase), but remains unchanged or even increased with electron doping ( $\delta$  decrease). This doping asymmetry can be explained by the different hopping probability of localized electrons ( $\text{Co}^{2+}$ ) and holes ( $\text{Co}^{4+}$ ) moving in the background of  $\text{Co}^{3+}$  ions because of the spin blockade of the electron transport [101]. At high temperatures, both compounds showed a small, negative, and almost temperature-independent and doping-independent Seebeck coefficient, which is quite natural for a metallic state. On the insulating side, on the other hand, the temperature dependences of the Seebeck coefficient were rather complicated and did not follow a simple  $\sim 1/T$  law expected for insulators. The thermo-e.m.f. value of  $\text{LnBaCo}_2\text{O}_{5+\delta}$  ( $\text{Ln} = \text{Nd}, \text{Gd}$ ) compounds depended strongly on the oxygen content and were positive for  $\delta > 0.5$  and negative for  $\delta < 0.5$  and reached maximal values around  $550 \mu\text{V} \cdot \text{K}^{-1}$  at 100 K for  $\delta \approx 0.5$ . The doping dependence of the thermo-e.m.f. values evinced that configurational entropy of charge carriers, enhanced by their spin and orbital degeneracy, plays a key role in the origin of the large thermoelectric response in these correlated oxides [101].

According to the [94], the  $\text{LnBaCo}_2\text{O}_6$  ( $\text{Ln} = \text{Nd}, \text{Sm}, \text{Eu}, \text{Gd}, \text{Tb}, \text{Dy}$ ) oxides demonstrate semiconductor to metal phase transition at temperature  $T = 330\text{--}360 \text{ K}$  (table 8), which value, in a whole, decreased at decreasing of  $\text{Ln}^{3+}$  ionic radius.

## 5.2. $\text{LnBaMe}'\text{Me}''\text{O}_{5+\delta}$ ( $\text{Ln} - \text{Y}, \text{REE}; \text{Me}', \text{Me}'' - \text{Fe}, \text{Co}, \text{Cu}$ ) phases

Authors of [102] had measured the low temperature (within 77–300 K) electrical resistivity of  $\text{PrBaFeCuO}_{5+\delta}$  ( $\delta = 0.00, 0.25$ ) samples. The stoichiometric sample ( $\text{PrBaFeCuO}_{5.00}$ ) presented values of the resistivity that at room temperature were five orders of magnitude higher than the oxygen-rich one ( $\text{PrBaFeCuO}_{5.25}$ ) ( $\approx 10^2 \Omega \cdot \text{m}$  and  $\approx 10^{-3} \Omega \cdot \text{m}$  respectively), this fact indicated that in the oxygen-rich sample the extra-oxygen is very important in the conduction mechanism. In the measured range of temperature, the oxygen-rich sample ( $\text{PrBaFeCuO}_{5.25}$ ) followed perfectly the expression (21):

$$\rho = \rho_0 \exp\left(\frac{T_0}{T}\right)^\nu \quad (21)$$

with  $\nu = 1/2$ . This is the expression for the general variable hopping conduction mechanism. Nevertheless, stoichiometric sample ( $\text{PrBaFeCuO}_{5.00}$ ) resistivity seemed to follow the expression for the variable range hopping but with an exponent  $\nu = 1/3$ , which had been proposed for planar conduction [103]. That change in the exponent could be explained because conduction in the stoichiometric sample is carried by variable range hopping and carriers moves in the  $-(\text{Fe},\text{Cu})\text{O}_2-$  planes; but when extra-oxygen are in the O3 sites (apical oxygen of both octahedral belonging to different  $-(\text{Fe},\text{Cu})\text{O}_2-$  planes), these  $-(\text{Fe},\text{Cu})\text{O}_2-$  planes are connected and the two dimensional conduction becomes destroyed [102].

On the electric properties all the  $\text{LnBaMe}'\text{Me}''\text{O}_{5+\delta}$  ( $\text{Ln} - \text{REE}; \text{Me}', \text{Me}'' - \text{Fe}, \text{Co}, \text{Cu}$ ) can be divided in two groups, namely group of La ( $\text{La-Nd}$ ) and group of Y ( $\text{Y}, \text{Gd-Lu}$ ), which  $\sigma = f(T)$  and  $S = f(T)$  dependences strongly differ (fig. 15). Electrical conductivity of oxygen-rich  $\text{LaBaMe}'\text{Me}''\text{O}_{5+\delta}$  phases at high temperatures changes its semiconducting character to metallic (fig. 15a) and the values

of Seebeck coefficient ( $S$ ) of these phases begins to increase (fig. 15c) due to the beginning of weakly-bound oxygen losses from the samples [63,104]. The maximal value of  $\sigma$  among the  $\text{LaBaMe}'\text{Me}''\text{O}_{5+\delta}$  phases has the  $\text{LaBaCoCuO}_{5+\delta}$  oxide but the minimal one does the  $\text{LaBaFeCuO}_{5+\delta}$  compound. The  $\text{YBaFeCoO}_{5+\delta}$  and  $\text{YBaCoCuO}_{5+\delta}$  phases possess the similar values of electrical conductivity at all temperatures studied and these values are one–two order of magnitude larger than  $\text{YBaFeCuO}_{5+\delta}$  perovskite (fig. 15b). The  $S = f(T)$  peak near 410 K for  $\text{YBaFeCoO}_{5+\delta}$  and near 475 K for  $\text{YBaCoCuO}_{5+\delta}$  (fig. 15d) is apparently due to the change in the spin state of cobalt cations like  $\text{Co}^{3+}$  spin transitions in the rare–earth elements cobaltites  $\text{LnCoO}_3$  [105]. Note that  $S$  values for  $\text{LaBaFeCoO}_{5+\delta}$  at  $T < 975$  K and for  $\text{LaBaCoCuO}_{5+\delta}$  within 600–900 K are negative but  $\text{LaBaFeCuO}_{5+\delta}$  and  $\text{YBaMe}'\text{Me}''\text{O}_{5+\delta}$  ( $\text{Me}'$ ,  $\text{Me}''$  – Fe, Co, Cu) compounds are the  $p$ –type semiconductors within all the temperatures studied (fig. 15c,d).

As can be seen from the fig. 16, all the oxides  $\text{LnBaMe}'\text{Me}''\text{O}_{5+\delta}$  ( $\text{Ln}$  – REE;  $\text{Me}'$ ,  $\text{Me}''$  – Fe, Co, Cu) are the  $p$ –type semiconductors (except above mentioned  $\text{LaBaFeCoO}_{5+\delta}$  and  $\text{LaBaCoCuO}_{5+\delta}$  compounds) and their  $\sigma$  values, in the whole, decrease but  $S$  values increase when lanthanide ionic radii increase. The  $\text{LnBaFeCoO}_{5+\delta}$  compounds had the larger values of  $\sigma$  ( $\sigma_{\text{max}} \approx 1.6 \cdot 10^4 \text{ S}\cdot\text{m}^{-1}$  near 650 K for  $\text{NdBaFeCoO}_{5+\delta}$  (fig. 16a)) but the  $\text{LnBaFeCrO}_{5+\delta}$  phases demonstrate the larger  $S$  values ( $S_{\text{max}} \approx 710\text{--}730 \mu\text{V}\cdot\text{K}^{-1}$  near 1050 K for  $\text{LnBaFeCuO}_{5+\delta}$  ( $\text{Ln}$  – Dy, Ho) (fig. 16b) and reach the value of  $1 \text{ mV}\cdot\text{K}^{-1}$  at 640 K for  $\text{TmBaFeCuO}_{5+\delta}$  [22]).

At high temperatures the electrical conductivity character of the ferrocobaltites and  $\text{LnBaFeCuO}_{5+\delta}$ ,  $\text{LaBaCoCuO}_{5+\delta}$  ( $\text{Ln}$  = La, Pr, and Nd) phases change from semiconducting ( $\partial\sigma/\partial T > 0$ ) to metallic ( $\partial\sigma/\partial T < 0$ ) (fig. 15a, 16a–c), while the  $S$  values started to rise sharply (fig. 15c, 16d–f). As it was mentioned above, this is caused by the evolution of the weakly–bonded oxygen ( $\delta$ ) from the crystal lattice of these compounds.

On the  $S = f(T)$  dependences for  $\text{LnBaFeCoO}_{5+\delta}$  oxides and  $\text{LnBaCoCuO}_{5+\delta}$  ( $\text{Ln}$  – Sm–Ho) phases the maximum near 350 K for  $\text{SmBaFeCoO}_{5+\delta}$ , 460 for  $\text{LnBaFeCoO}_{5+\delta}$  ( $\text{Ln}$  = Gd, Dy, Ho), 500 K for  $\text{SmBaCoCuO}_{5+\delta}$  and at 495–510 K for  $\text{LnBaCoCuO}_{5+\delta}$  ( $\text{Ln}$  = Gd, Dy, Ho) is observed (fig. 16d,f). The  $S$  values increasing for these phases in the low-temperature region is caused to the change in the spin state of the cobalt cations  $\text{Co}^{3+}$ ,  $\text{Co}^{4+}$  in their crystal structure from intermediate–spin (IS) into the high–spin state (HS)  $\text{Co}_{\text{IS}}^{3+} (t_{2g}^5 e_g^1) \rightarrow \text{Co}_{\text{HS}}^{3+} (t_{2g}^4 e_g^2)$ ,  $\text{Co}_{\text{IS}}^{4+} (t_{2g}^4 e_g^1) \rightarrow \text{Co}_{\text{HS}}^{4+} (t_{2g}^3 e_g^2)$  similarly to the spin state transition of the  $\text{Co}^{3+}$  cations in the perovskite REE cobaltites  $\text{LnCoO}_3$  [105].

The  $\text{LnBaMe}'\text{Me}''\text{O}_{5+\delta}$  ( $\text{Ln}$  – REE;  $\text{Me}'$ ,  $\text{Me}''$  – Fe, Co, Cu) layered perovskites are the materials with polaronic transport and their temperature dependences of electrical conductivity and Seebeck's coefficient can be described by the relations (22,23):

$$\sigma = A/T \cdot \exp\left(-E_A/k_B T\right) \quad (21)$$

$$S = \pm k_B/e \left(-E/k_B T + B\right) \quad (21)$$

where  $E_A = E + W$  is the activation energy of electrical conductivity,  $E$  is the excitation energy of the charge transfer (polarons), but  $W$  is their transport energy ( $W \approx 0$  for non–activated charge transport by large polarons (LP); if  $W > 0$ , charge transport is thermally activated and is due to the small–polaron (SP) hopping [106].

The values of  $E$  and  $W$  determined from the linear parts of the plots  $\ln(\sigma T) = f(1/T)$  and  $S = f(1/T)$  for the oxides  $\text{LnBaMe}'\text{Me}''\text{O}_{5+\delta}$  ( $\text{Ln}$  – REE;  $\text{Me}'$ ,  $\text{Me}''$  – Fe, Co, Cu) are given in the table 9. As can

be seen, the charge carriers in the  $LnBaMe'Me''O_{5+\delta}$  phases are the small polarons ( $W > 0$ ), but for  $LnBaCoCuO_{5+\delta}$  ( $Ln - Dy, Ho$ ) above 775 K (for  $Ln - Dy$ ) and 530 K ( $Ln - Ho$ ) the charge carriers are the large polarons ( $W \approx 0$ ). As can be seen from the table 9, the values of activation energy of electrical transport ( $E_A$ ,  $E$  and  $W$ ) in the  $LnBaMe'Me''O_{5+\delta}$  compound, as a whole, increase when lanthanide ionic radii decrease.

Table 9. Values of activation energies of transport processes ( $E_A$ ,  $E$ ,  $W$ ) for the layered perovskites  $LnBaMe'Me''O_{5+\delta}$  ( $Ln - Y, REE; Me', Me'' - Fe, Co, Cu$ ) for different temperature regions

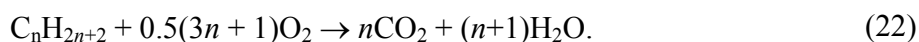
Compound	$E_A$ , eV	$E$ , eV	$W$ , eV	$T$ , K	Ref.
1	2	3	4	5	6
YBaFeCoO <sub>5+δ</sub>	0,345	0,046	0,299	410–600	[59]
		0,097	0,248	600–780	
YBaCoCuO <sub>5+δ</sub>	0,352	0,168	0,184	480–1050	[66]
YBaCoCuO <sub>5+δ</sub>	0,14	–	–	320–390	[87]
	0,39	–	–	390–795	
	0,25	–	–	795–1050	
YBaFeCuO <sub>5+δ</sub>	0,240	–	–	300–1100	[60]
LaBaFeCoO <sub>5+δ</sub>	0,087	0,006	0,081	300–670	[63]
LaBaCoCuO <sub>5+δ</sub>	0,042	0,021	0,021	300–670	[63]
LaBaFeCuO <sub>5+δ</sub>	0,061	–	–	300–600	[60]
PrBaFeCoO <sub>5+δ</sub>	0,126	0,016	0,110	350–610	[64]
		0,053	0,073	610–750	
PrBaCoCuO <sub>5+δ</sub>	0,097	0,042	0,055	530–750	[64]
PrBaFeCuO <sub>5+δ</sub>	0,126	–	–	300–600	[60]
NdBaCoCuO <sub>5+δ</sub>	0,080	0,009	0,071	320–630	[61]
NdBaFeCuO <sub>5+δ</sub>	0,201	–	–	300–800	[60]
	0,112	–	–	800–1100	
SmBaCoCuO <sub>5+δ</sub>	0,364	0,194	0,170	510–1050	[61]
SmBaFeCuO <sub>5+δ</sub>	0,289	–	–	300–750	[60]
	0,221	–	–	750–1100	
EuBaFeCuO <sub>5+δ</sub>	0,314	–	–	300–650	[60]
	0,210	–	–	650–1000	
GdBaCoCuO <sub>5+δ</sub>	0,371	0,121	0,250	370–1050	[61]
GdBaFeCuO <sub>5+δ</sub>	0,319	–	–	300–1100	[60]
TbBaFeCoO <sub>5+δ</sub>	0,384	0,066	0,318	460–590	[59]
		0,184	0,200	590–860	
TbBaFeCuO <sub>5+δ</sub>	0,213	–	–	300–450	[60]
	0,385	–	–	450–1000	
DyBaFeCoO <sub>5+δ</sub>	0,374	0,033	0,341	460–580	[59]
		0,106	0,268	580–800	
DyBaCoCuO <sub>5+δ</sub>	0,285	0,133	0,152	480–775	[66]
		0,282	0,003	775–1050	
DyBaFeCuO <sub>5+δ</sub>	0,373	–	–	300–1100	[60]
HoBaFeCoO <sub>5+δ</sub>	0,359	0,022	0,337	460–530	[59]
		0,076	0,283	530–750	
HoBaCoCuO <sub>5+δ</sub>	0,257	0,135	0,124	500–800	[69]
		0,254	0,003	800–1100	
HoBaFeCuO <sub>5+δ</sub>	0,194	–	–	300–600	[60]
	0,274	–	–	600–900	
	0,458	–	–	900–1100	
ErBaFeCuO <sub>5+δ</sub>	0,517	–	–	500–1000	[60]
TmBaFeCuO <sub>5+δ</sub>	0,637	–	–	300–1000	[60]

1	2	3	4	5	6
YbBaFeCuO <sub>5+δ</sub>	0,251	–	–	400–1000	[60]
LuBaFeCuO <sub>5+δ</sub>	0,323	–	–	300–600	[60]
	0,383	–	–	600–900	
	0,531	–	–	900–1100	

Fig. 17 shows strong dependence of electric conductivity and thermo-e.m.f. of PrBaFeCuO<sub>5+δ</sub> from value of its oxygen non-stoichiometry index. As can be seen from the fig. 17a, the conductivity mechanism of PrBaFeCuO<sub>5+δ</sub> remains unchanged when δ decreases but activation energy of electrical conductivity, calculated from equation (21), increases from 0.15 eV for sample with δ = 0.28 to 0.30 eV for fully reduced sample PrBaFeCuO<sub>5,00</sub> [89]. When oxygen content in the PrBaFeCuO<sub>5+δ</sub> decreases the  $S = f(T)$  dependences change drastically and the  $S$  values strongly decrease reaching value around 400 μV·K<sup>-1</sup> for PrBaFeCuO<sub>5,00</sub> compound near 470 K (fig. 17b).

## 6. Catalytic, sensor, thermoelectric and other properties

The catalytic activity of the YBaFe<sub>0,9</sub>Me<sub>0,1</sub>CuO<sub>5+δ</sub> (Me = Mn, Fe, Co, Ni) compounds had been tested in reaction of oxidation of hydrocarbons by atmospheric oxygen:



The green YBaFe<sub>0,9</sub>Me<sub>0,1</sub>CuO<sub>5+δ</sub> powders were formed into granules using organic binding and these granules was annealed at 773 K for 5 h for firing of organics and then sintered at 1273 K for 1 h. The specific area of the granules determined using low-temperature BET adsorption method was about 2.2–3.9 m<sup>2</sup>·g<sup>-1</sup> [15]. These granules were put into quartz tube and through this tube the flow of hydrocarbons mixture with air (hydrocarbons content was 0.1–0.2 vol. %) were passed at volume rate 2.4–3.6·10<sup>4</sup> h<sup>-1</sup> at temperatures up to 1100 K. The composition of gas mixture after passing it through the tube with and without the catalyst was determined using chromatography. For the catalytic activity measure of YBaFe<sub>0,9</sub>Me<sub>0,1</sub>CuO<sub>5+δ</sub> compounds the conversion degree of hydrocarbons (α) after reaction (22) was taken [15]. As can be seen from the fig. 18, the YBaFe<sub>0,9</sub>Me<sub>0,1</sub>CuO<sub>5+δ</sub> showed appreciable catalytic activity (α > 10%) in reaction (22) at temperature around 623 K and the full conversion of propane–butane mixture by atmospheric oxygen in the presence of catalysts with YBaFe<sub>0,9</sub>Me<sub>0,1</sub>O<sub>5+δ</sub> (Me – Co, Ni) composition was observed at 983 K.

The possibility of using of LnBaFe<sub>0,9</sub>Me<sub>0,1</sub>CuO<sub>5+δ</sub> (Ln – La, Y; Me – Mn, Fe, Co, Ni) oxides as materials for semiconducting gas sensors had been investigate in [6,16]. The thick films ( $d \approx 2\text{--}5 \mu\text{m}$ ) of LnBaFe<sub>0,9</sub>Me<sub>0,1</sub>CuO<sub>5+δ</sub> were prepared by means of stencil printing from aqueous suspensions on the (Ca,La)(Ti,Al)O<sub>3</sub> polycrystalline substrate with following annealing at 1173–1223 K for 2–5 h in air. The sensitivity of these materials to the presence in air of gases-reducers admixtures (hydrocarbons, alcohols, ammonia etc.) at content of these gases on the level 10<sup>-1</sup>–10<sup>5</sup> ppm (10<sup>-5</sup>–10 vol.%) had been measured. The value of the sensor response (ε) had been calculated as (23):

$$\varepsilon = \frac{(R_g - R_0)}{R_0} \cdot 100\%, \quad (23)$$

where  $R_g$  and  $R_0$  were the resistance values of the films studied in atmosphere with and without of the gas-reducer, respectively.

It was found [6,16] that the LnBaFe<sub>0,9</sub>Me<sub>0,1</sub>CuO<sub>5+δ</sub> compounds demonstrated a significant sensitivity to the presence in air of various oxygen-containing gases-reducers (ethanol, dioxane etc.) did not showed practically response to the presence in air of various hydrocarbons. The maximal

response value was obtained near 650–700 K for the compositions with Me = Mn, Ni which response consisted up to 250% at content of the analyzed gas in atmosphere on the level of  $\approx 10^2$  ppm (fig. 19).

On the base of the compositions which had showed the maximal sensitivity at detection of analyzed gases in air the working elements of chemical gas sensors were produced. The schema of the typical working element is done on the fig. 20. The value of power of heater was changed within 100–600 W. The maximal response values of the gas sensors produced were obtained when power of heater was about 200–300 mW (fig. 21) hereby the sensitivity as well as the selectivity of working elements studied were large than for the thick films ones. As can be seen from the fig. 22, the YBaCuFe<sub>0.8</sub>Ni<sub>0.2</sub>O<sub>5</sub>-based gas sensor demonstrates large threshold sensitivity (10 ppm) to the presence of ethanol vapours in atmosphere, the large slope of signal dependence on analyzed gas content (within  $10^1$ - $10^4$  ppm) and can be used for detection of ethanol in air.

The good thermoelectric materials should possess simultaneously the high values of electrical conductivity ( $\sigma$ ) and Seebeck coefficient ( $S$ ) and low values of thermal conductivity ( $\kappa$ ) to provide the large values of thermoelectric efficiency ( $Z$ ) and power factor ( $P$ ):

$$Z = \frac{S^2 \sigma}{\kappa} = \frac{P}{\sigma}, P = S^2 \sigma, \quad (24)$$

which characterize the efficiency of heat into electrical energy transformation ( $Z$ ) and efficiency of the charge transfer in the thermoelectric materials.

As it was mentioned above in this chapter (section 5), the some of  $LnBaMe'Me''O_{5+\delta}$  ( $Ln$  – REE; Me – Fe, Co, Cu) layered oxides possess the high values of electrical conductivity and thermopower, so they have to be probed as perspective thermoelectric materials. It should be note that oxide thermoelectric materials have advantages for high-temperature operation in air where they are more stable than conventional thermoelectrics, such us Bi<sub>2</sub>Te<sub>3</sub>, Sb<sub>2</sub>Te<sub>3</sub> etc. [107].

The power factor values ( $P$ ) calculated using the experimental  $\sigma$  and  $S$  values for the  $LnBaMe'Me''O_{5+\delta}$  oxides are given on the fig. 23. As can be seen, the  $P$  values for these oxides, in the whole, increase at temperature increasing and strongly depend on the nature of the REE and  $3d$ -metals in their crystal structure. Peak  $P$  values (among the oxides described in this chapter) were observed for PrBaFeCuO<sub>5+\delta</sub>, SmBaCuFeO<sub>5+\delta</sub>, and NdBaCoFeO<sub>5+\delta</sub>: 137, 63,0 and 39,2  $\mu W \cdot m^{-1} \cdot K^{-2}$  respectively at  $T = 1050$  K. Though these values are considerably smaller than power factor values for the sodium-cobalt oxide bronzes (for NaCo<sub>1.8</sub>Cu<sub>0.2</sub>O<sub>4</sub>, for example, at 1073 K  $P = 3.08$   $mW \cdot m^{-1} \cdot K^{-2}$  [4]), but they are closed to the  $P$  values for ceramic based on Ca<sub>3</sub>Co<sub>2</sub>O<sub>6</sub> (for (Ca,Bi)<sub>3</sub>(Co,Cu)<sub>2</sub>O<sub>6</sub> solid solutions  $P \approx 30$ – $50$   $\mu W \cdot m^{-1} \cdot K^{-2}$  near 1173 K [5,6] and for Ca<sub>2.85</sub>Er<sub>0.15</sub>Co<sub>2</sub>O<sub>6</sub> phases  $P = 10.66$   $\mu W \cdot m^{-1} \cdot K^{-2}$  at  $T = 1073$  K [7]) and LaCoO<sub>3</sub> (for LaCo<sub>0.80</sub>Ti<sub>0.20</sub>O<sub>2.86</sub> and LaCo<sub>0.80</sub>Ni<sub>0.20</sub>O<sub>2.95</sub> power factor values are 28.2 and 9.5  $\mu W \cdot m^{-1} \cdot K^{-2}$  respectively at 1243 K [12]).

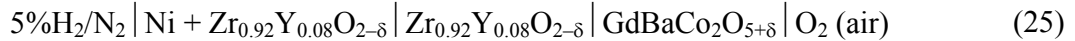
Thus, the layered compounds  $LnBaMe'Me''O_{5+\delta}$ , principally, may be used as a base for development of the new thermoelectric oxide materials.

The high value of electrical conductivity of  $LnBaCo_2O_{5+\delta}$  phases and presence in their crystal structure of weakly-bound oxygen ( $\delta$ ) allow to consider them as promising materials of cathodes of solid oxide fuel cells (SOFC) and oxygen permeation membranes.

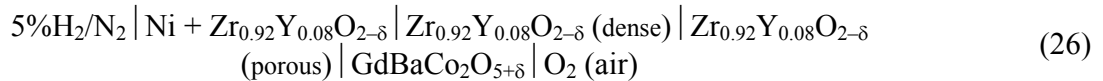
So, in [17] the electrode performance of GdBaCo<sub>2</sub>O<sub>5+\delta</sub> cobaltite had been investigated at temperatures below 973 K by AC impedance spectroscopy. The lowest area surface resistance (ASR) had been measured for GdBaCo<sub>2</sub>O<sub>5+\delta</sub>/Ce<sub>0.8</sub>Gd<sub>0.2</sub>O<sub>2-\delta</sub> sample sintered at 1173 K and it consisted 0.53  $\Omega \cdot cm^2$  at 918 K. The total ASR was found to be large when the electrode was sintered at 1073 K and this was attributed to poor adhesion of the cathode layers. It was noticeable that there was little performance degradation on increasing the sintering temperature from 1173 K to 1273 K, but a further increase to 1323 K resulted in significant performance degradation (increase of ASR values). Note that

the activation energy values for the electrode behavior on  $\text{Ce}_{0.8}\text{Gd}_{0.2}\text{O}_{2-\delta}$  solid electrolyte, calculated from  $\ln(1/R) = f(1/T)$  dependences, did not show significant variation with sintering conditions and were 1.27 eV, 1.34 eV and 1.21 eV for the cathodes sintered at 1173 K, 1273 K and 1323 K, respectively. The obtained in [17] results indicate that  $\text{GdBaCo}_2\text{O}_{5+\delta}$  is a promising cathode material for intermediate temperature solid oxide fuel cells (ITSOFCs).

Authors [18] using  $\text{GdBaCo}_2\text{O}_{5+\delta}$  as cathode material, had constructed the cell:



and measured its voltage and power density as a function of current density from 873 to 1073 K. The power density of the cell (25) increased with increasing the operating temperature. The maximal power density values of the cell were  $250 \text{ mW}\cdot\text{cm}^{-2}$  and  $150 \text{ mW}\cdot\text{cm}^{-2}$  at 1073 K and 973 K respectively. In order to improve the power density of cell the intermediate porous layer of  $\text{Zr}_{0.92}\text{Y}_{0.08}\text{O}_{2-\delta}$  was put between solid electrolyte ( $\text{Zr}_{0.92}\text{Y}_{0.08}\text{O}_{2-\delta}$ ) and cathode ( $\text{GdBaCo}_2\text{O}_{5+\delta}$ ). The maximal power density values for improved cell were  $550 \text{ mW}\cdot\text{cm}^{-2}$  and  $300 \text{ mW}\cdot\text{cm}^{-2}$  at 1173 K and 973 K, respectively. The maximum power densities at 1073 K was close to the often-considered target value of  $500 \text{ mW}\cdot\text{cm}^{-2}$  for technological applications [18]. These results indicate that the SOFC system (26):



produced in [18], represents an excellent candidate for intermediate temperature applications.

The oxygen permeability and cathode performance of  $\text{LnBaCo}_2\text{O}_{5+\delta}$  ( $\text{Ln} - \text{La, Pr, Nd, Sm, Gd}$  and  $\text{Y}$ ) compounds had been studied in [19]. It was found that  $\text{PrBaCo}_2\text{O}_{5+\delta}$  demonstrated the highest oxygen flux ( $\sim 5.09 \cdot 10^{-7} \text{ mol}\cdot\text{cm}^{-2}\cdot\text{s}^{-1}$  at 1173 K), but this value was still significantly lower than that of  $\text{Ba}_{0.5}\text{Sr}_{0.5}\text{Co}_{0.8}\text{Fe}_{0.2}\text{O}_{3-\delta}$  perovskite ( $\sim 3.01 \text{ mol}\cdot\text{cm}^{-2}\cdot\text{s}^{-1}$  at 1173 K). The observed difference was attributed to the much longer diffusion distance through a polycrystalline membrane with a layered lattice structure than through cubic perovskite because bulk diffusion was the rate-limiting stage of permeation. Attractive high electrode performance (using  $\text{Sm}_{0.2}\text{Ce}_{0.8}\text{O}_{1.9}$  solid electrolyte), however, was observed for  $\text{LnBaCo}_2\text{O}_{5+\delta}$  oxides, especially  $\text{PrBaCo}_2\text{O}_{5+\delta}$ , which possessed an area-specific resistance of  $\sim 0.213 \Omega\cdot\text{cm}^2$  at 873 K. These results suggest that these layered cobaltites might be best applied as materials for reduced-temperature SOFC electrodes rather than as materials for ceramic oxygen-separation membranes.

The electrochemical performance of layered oxides  $\text{LaBaMeCuO}_{5+\delta}$  ( $\text{Me} - \text{Fe, Co}$ ) had been investigated as potential cathode materials for ITSOFCs [20]. It had been found that electrical conductivity of  $\text{LaBaCuCoO}_{5+\delta}$  was much higher than that of  $\text{LaBaCuFeO}_{5+\delta}$ . Area specific resistances of  $\text{LaBaCuFeO}_{5+\delta}$  and  $\text{LaBaCuCoO}_{5+\delta}$  cathode materials on  $\text{Ce}_{0.8}\text{Sm}_{0.2}\text{O}_{1.9}$  solid electrolyte were as low as  $0.21 \Omega\cdot\text{cm}^2$  and  $0.11 \Omega\cdot\text{cm}^2$  at 973 K, respectively. The maximum power density of the cells (27)



with 300  $\mu\text{m}$  thick electrolytes attains  $557 \text{ mW cm}^{-2}$  and  $603 \text{ mW cm}^{-2}$  at 1073 K for  $\text{Me} = \text{Fe}$  and  $\text{Co}$ , respectively [20]. These results demonstrated that the layered perovskite-structure oxides  $\text{LaBaMeCuO}_{5+\delta}$  ( $\text{Me} - \text{Fe, Co}$ ) are very promising cathode materials for application in ITSOFCs.

## 7. Conclusion

In this chapter the preparation methods, crystal structure and thermal stability of layered  $\text{LnAME}_2\text{O}_{5+\delta}$  ( $\text{Ln} - \text{REE}$ ;  $\text{A} - \text{AE, AEE}$ ;  $\text{Me} - 3d\text{-metal}$ ) double perovskites are described as well as their thermal expansion, magnetic, electrical and other properties are discussed. It is shown that the

REE and 3d-metal nature as well as the oxygen sub-lattice state (including oxygen content) of the samples strongly influence on their crystal structure and properties.

The various nature (structural, electrical, magnetic) phase transitions taking place in these oxides in a wide temperature range are described. So, layered manganites  $LnBaMn_2O_{5+\delta}$  and cobaltites  $LnBaCo_2O_{5+\delta}$  demonstrate a number of magnetic transitions due to the various type ordering of magnetic ions (manganese or cobalt) in their structure, but layered ferrites  $LnBaFe_2O_{5+\delta}$  show transition of Verwey type due to dis-proportionation of valence-mixed state of iron ions ( $Fe^{+2.5}$ ) into charge-ordered state of the ones ( $Fe^{2+}$  and  $Fe^{3+}$ ).

It is shown that large values of electrical conductivity and thermo-e.m.f values of some  $LnBaMe_2O_{5+\delta}$  phases and presence in their structure of the weakly-bound (labile) oxygen causes possibility of their usage as materials for semiconducting chemical sensors of gases and oxidation catalysts of hydrocarbons ( $LnBaFeCuO_{5+\delta}$  oxides), cathode materials for intermediate temperature solid oxide fuel cells ( $LaBaMeCoO_{5+\delta}$  (Me – Fe, Cu) compounds and  $LnBaCo_2O_{5+\delta}$  phases) or materials for high-temperature conversion of heat into electrical energy in thermoelectric generators ( $LnBaFeMeO_{5+\delta}$  (Me – Co, Cu) oxides).

## 8. References

1. V'yunov, O.I.; Kovalenko, L.L.; Belous, A.G.; Belyakov, V.N. *Inorg. Mater.* 2005, *41*, 87-94.
2. Tretyakov, Yu.D.; Goodilin, E.A. *Rus Chem Rev* 2000, *69*, 1-34.
3. Gorelov, V.P.; Balakireva, V.B.; Kleshchev, Yu.N.; Brusentsov, V.P. *Inorg. Mater* 2001, *37*, 535-538.
4. Huang, K.; Tichy, S.; Goodenough, J.B. *J. Amer. Ceram. Soc.* 1998, *81*, 2565-2575.
5. Peña, M.A.; Fierro, J.L.G. *Chem. Rev.* 2001, *101*, 1981-2017.
6. Klyndziuk, A.; Petrov, G.; Kurhan, S.; Chizhova, Ye.; Chabatar, A.; Kunitski, L.; Bashkirov, L. *Chem. Sensors*, 2004, *20 (Suppl. B)*, 854-855.
7. Michel, C.R.; Delgado, E.; Santillan, G.; Martinez, A.H.; Chavez-Chavez, A. *Mat. Res. Bull.* 2007, *42*, 84-93.
8. Rao, C.N.R.; Cheetham, A.K.; Mahesh R. *Chem. Mater.* 1996, *8*, 2421-2432.
9. Robert, R.; Bocher, L.; Trottmann, M.; Reller, A.; Weidenkaff, A. *J. Solid State Chem* 2006, *179*, 3893-3899.
10. Yasukawa, M.; Murayama, N. *Mat. Sci. Eng. B* 1998, *54*, 64-69.
11. West, A. *Solid State Chemistry and Its Applications.*; John Wiley & Sons: Chichester-New York-Brisbane-Toronto-Singapore, DE, 1985, 204-207.
12. Er-Rakho, L.; Michel, C.; LaCorre, Ph.; Raveau, B. *J. Solid State Chem.* 1988, *73*, 531-535.
13. Nakajima, T.; Kageyama, H.; Ichihara, M.; Ohoyama, K.; Yoshizawa, H.; Ueda, Y. *J. Solid State Chem.* 2004, *177*, 987-999.
14. Streule, S.; Podlesnyak, A.; Sheptyakov, D.; Pomjakushina, E.; Stingaciu, M.; Conder, K.; Medarde, M.; Patrakee, M.V.; Leonidov, I.A.; Kozhevnikov, V.L.; Mesot, *J. Phys. Rev. B.* 2006, *73*, 094203 (5 pp).
15. Chizhova, Ye.; Klyndyuk, A.; Petrov, G.; Shvaro A.; Kurhan, S.; Bashkirov, L. MSU-HTSC VII, June 20-25 2004, Moscow. P4.
16. Klyndyuk, A.I., Chizhova, Ye.A.; Taratyn, I.A. *Trudy BGTU, Ser III Khim Technol Neorg Veshch*, 2005, III, 54-58.
17. Chang, A.; Skinner, S.J.; Kilner, J.A. *Solid State Ionics* 2006, *177*, 2009-2011.
18. Tarascon, A.; Morata, A.; Dezanneau, G.; Skinner, S.J.; Kilner, J.A.; Estrade, S.; Hernandez-Ramirez, F.; Peiro, F.; Morante, J.R. *J. Power Sources* 2007, *174*, 255-263.
19. Zhang, K.; Ge, L.; Ran, R.; Shao, Z.; Liu, S. *Acta Materialia* 2008, *56*, 4876-4889.
20. Zhou, Q.; He, T.; He, Q.; Ji, Yu. *Electrochem. Commun.* 2009, *11*, 80-83.
21. Klyndyuk, A.I.; Chizhova, Ye.A. *Funct. Mater.* 2009, *16*, 17-22.
22. Klyndyuk, A.I. *Phys. Solid State* 2009, *51*, 250-254.
23. Ramesha, K.; Smolyaninova, N.V.; Gopalakrishnan, J.; Greene, R.L. *Chem. Mater.* 1998, *10*, 1436-1439.
24. Davrenbekov, S.Zh.; Mustafin, E.S.; Kasenov, B.K.; Edil'baeva, S.T.; Kasenova, Sh.B.; Zhumadilov, E.K., Sagintaeva, Zh.I. *Inorg. Mater* 2004, *40*, 976-978.
25. Trukhanov, S.V.; Troyanchuk, I.O.; Hervieu, M.; Szymczak, H.; Bäerner, K. *Phys. Rev. B.* 2002, *66*, 184424 (10 pp).
26. Beales, T.P.; Möllg, M.; Jutson, J. *J. Mat. Sci. Lett.* 1997, *16*, 663-664.
27. Karen, P. *J. Solid State Chem.* 2004, *177*, 281-292.
28. Roy, S.; Dubenko, I.S.; Khan, M.; Condon, E.M.; Craig, J.; Ali, N. *Phys. Rev. B* 2005, *71*, 024419 (8 pp).
29. Sun, W.; Bi, L.; Yan, L.; Peng, R.; Liu, W. *J. Alloys Comp.* 2009, *481*, L40-L42.

30. Kasenov, B.K.; Davrenbekov, S.Zh.; Mustafin, E.S.; Kasenova, Sh.B.; Edil'baeva, S.T.; Zhumadilov, E.K. *Inorg. Mater* 2006, 42, 68–74.
31. Davrenbekov, S.Zh.; Edil'baeva, S.T.; Kasenov, B.K.; Mustafin, E.S.; Zhumadilov, E.K.; Kasenova, Sh.B. *Rus. J. Inorg. Chem.* 2005, 50, 516–520.
32. Kasenov, B.K.; Edil'baeva, S.T.; Mustafin, E.S.; Kasenova, Sh.B.; Zhumadilov, E.K.; Davrenbekov, S.Zh. *Rus. J. Inorg. Chem.* 2003, 48, 1306–1309.
33. Davrenbekov, S.Zh.; Kasenov, B.K.; Zhumadilov, E.K.; Mustafin, E.S.; Kasenova, Sh.B.; Edil'baeva, S.T. *Rus. J. Inorg. Chem.* 2004, 49, 264–268.
34. Chapman, J.P.; Attfield, J.P.; Mölgg, M.; Friend, C.M.; Beales, T.P. *Angew. Chem. (Eng. Ed.)* 1996, 35, 2482–2484.
35. Beales, T.P.; Mölgg, M.; Jutson, J.; Friend, C.M. *Phys. Stat. Sol. (a)* 1997, 161, 271–282.
36. Millange, F.; Suard, E.; Caignaert, V.; Raveau, B. *Mat. Res. Bull.* 1999, 34, 1–9.
37. Williams, A.; Attfield, J.P. *Phys. Rev. B* 2005, 72, 024436 (5 pp).
38. Nakajima, T.; Kageyama, H.; Ueda, Yu. *J. Phys. Chem. Solids* 2002, 63, 913–916.
39. Мустафин, Е.С.; Касенов, Б.К.; Едилбаева, С.Т. *Журн. неорганической химии* 2000, 45, 98.
40. Caignaert, V.; Millange, F.; Domenges, B.; Raveau, B. *Chem. Mater.* 1999, 11, 930–938.
41. Касенов, Б.К.; Оралова, А.Т.; Мустафин, Е.С.; *Журн. неорганической химии* 1998, 43, 1420–1421.
42. Mustafin, E.S.; Mataev, M.M.; Nurgaliev, B.Z.; Kasenov, B.K. *Neorg. Mater [in rus.]* 1994, 30, 140–144.
43. Kasenov, B.K.; Mustafin, E.S.; Kasenova, Sh.B.; Edil'baeva, S.T.; Tolokonnikov, E.G. *Rus. J. Inorg. Chem.* 2004, 49, 102–106.
44. Karen, P.; Woodward, P.M.; Santosh, P.N.; Vogt, T.; Stephens, P.W.; Pagola, S. *J. Solid State Chem.* 2002, 167, 480–493.
45. Linden, J.; Karen, P.; Kjekshus, A.; Miettinen, J.; Pietari, T.; Karppinen, M. *Phys. Rev. B.* 1999–II, 60, 15 251–15 260.
46. Kasenov, B.K.; Tolokonnikov, E.G.; Mustafin, E.S.; Kasenova, Sh.B.; Davrenbekov, S.Zh.; Sagintaeva, Zh.I.; Zhumadilov, E.K. *Rus. J. Inorg. Chem* 2006, 51, 368–373.
47. Akahoshi, D.; Ueda, Y. *J. Solid State Chem.* 2001, 156, 355–363.
48. Aurelio, G.; Curiale, J.; Sanchez, R.D. *Physica B* 2006, 384, 106–109.
49. Troyanchuk, I.O.; Kasper, N.V.; Khalyavin, D.D.; Chobot, A.N.; Chobot, G.M.; Szymchak, H. *J. Phys.: Condens. Matter.* 1998, 10, 6381–6389.
50. Moth Seikh, Md.; Caignaert, V.; Pralong, V.; Simon, Ch.; Raveau, B. *J. Phys.: Condens. Matter* 2008, 20, 015212 (7 pp).
51. Leonidov, I.A.; Patrakeev, M.V.; Mitberg, E.B.; Leonidova, O.N.; Kozhevnikov, V.L. *Inorg. Mater* 2006, 42, 196–201.
52. Moth Seikh, Md.; Caignaert, V.; Pralong, V.; Raveau, B. *Solid State Commun.* 2009, 149, 697–702.
53. Frontera, C.; Garcia-Muñoz, J.L.; Carrillo, A.E.; Aranda, M.A.G.; Margiolaki, I.; Caneiro, A. *Phys. Rev. B* 2006, 74, 054406 (11 pp).
54. Kim, W.S.; Chi, E.O.; Choi, H.S.; Nur, N.H.; Oh, S.-J.; Ri, H.-C. *Solid State Commun.* 2000, 116, 609–614.
55. Moritomo, Y.; Akimoto, T.; Takeo, M.; Machida, A.; Nishibori, E.; Takata, M.; Sakata, M.; Ohoyama, K.; Nakamura, A. *Phys. Rev. B.* 2000–II, 61, R13 325–R13 328.
56. Plakhty, V.P.; Chernenkov, Yu.P.; Barilo, S.N.; Podlesnyak, A.; Pomjakushina, E.; Moskvina, E.V.; Gavrilo, S.V. *Phys. Rev. B* 2005, 71, 214407 (14 pp).
57. Burley, J.C.; Mitchell, S.; Short, S.; Miller, D.; Tang, Y. *J. Solid State Chem.* 2003, 170, 339–350.
58. Karen, P.; Suard, E.; Fauth, F.; Woodward, P.M. *Solid State Sci.* 2004, 6, 1195–1204.
59. Klyndyuk, A.I.; Chizhova, E.A. *Phys. Solid State* 2009, 51, 657–661.
60. Klyndyuk, A.I.; Chizhova, E.A. *Inorg. Mater.* 2006, 42, 550–561.
61. Klyndyuk, A.I.; Chizhova, E.A. *Rus. J. Inorg. Chem.* 2009, 54, 1009–1013.
62. Huang, Q.; Karen, P.; Kjekshus, A.; Lynn, J.W.; Mighell, A.D.; Natali Sora, I.; Rosov, N.; Santoro, A. *J. Solid State Chem.* 1994, 108, 80–86.
63. Klyndyuk, A.I. *Phys. Solid State* 2009, 51, 270–274.
64. Klyndyuk, A.I. *Inorg. Mater.* 2009, 45, 942–945.
65. Rentshler, T. *J. Alloys Comp.* 1996, 232, 43–52.
66. Klyndyuk, A.I. *Rus. J. Inorg. Chem.* 2009, 54, 1014–1017.
67. Ruiz-Gonzalez, L.; Boulahya, K.; Parras, M.; Alonso, J.; Gonzalez-Calbet, J.M. *Chem. Eur. J.* 2002, 8, 5694–5700.
68. Suescun, L.; Jones, C.Y.; Cardoso, C.A.; Lynn, J.W.; Toby, B.H.; Araujo-Moreira, F.M.; de Lima, O.F.; Pardo, H.; Momburu, A.W. *Phys. Rev. B.* 2005, 71, 144405 (9 pp).
69. Klyndyuk, A.I. *Inorg. Mater.* 2009, 45, 806–808.
70. Meyer, C.; Hartmann-Boutron, F.; Gros, Y.; Strobel, P. *Solid State Commun.* 1990, 76, 163–168.
71. Linden, J.; Kochi, M.; Lehmus, K.; Pietari, T.; Karppinen, M.; Yamauchi, H. *J. Solid State Chem.* 2002, 166, 118–127.

72. Ruiz-Aragon, M.J.; Moran, E.; Amador, U.; Martinez, J.L.; Ehrenberg, H. *Phys. Rev. B.* 1998–II, 58, 6291–6297.
73. Mombro, A.W.; Christides, C.; Lappas, A.; Prassides, K.; Pissas, M.; Mitros, C.; Niarchos, D. *Inorg. Chem.* 1994, 33, 1255–1258.
74. Nagase, M.; Linden, J.; Miettinen, J.; Karppinen, M.; Yamauchi, H. *Phys. Rev. B.* 1998–II, 58, 3371–3376.
75. Pissas, M.; Mitros, C.; Kallias, G.; Psykharis, V.; Simopoulos, A.; Kostikas, A.; Niarchos, D. *Physica C* 1994, 192, 35–40.
76. Ruiz-Aragon, M.J.; Amador, U.; Moran, E.; Andersen, N.H. *Physica C* 1994, 235–240, 1609–1610.
77. Kallias, G.; Pissas, M.; Christides, C.; Sonntag, R.; Niarchos, D. *Physica B* 1997, 234, 608–610.
78. Er-Rakho, L.; Michel, C.; Studer, F.; Raveau, B. *J. Phys. Chem. Solids* 1987, 48, 377–382.
79. Er-Rakho, L.; Nguyen, N.; Ducouret, A.; Samdi, A.; Michel, C. *Solid State Sci* 2005, 7, 165–172.
80. Mombro, A.W.; Pardo, H.; Suescun, L.; Toby, B.H.; Ortiz, W.A.; Negreira, C.A.; Araujo-Moreira, F.M. *Physica C* 2001, 356, 149–159.
81. Pissas, M.; Kallias, G.; Psykharis, V.; Gamari-Seale, H.; Niarchos, D.; Simopoulos, A. *Phys. Rev. B* 1997–I, 55, 397–408.
82. Mombro, A.W.; Marimon da Cunha, J.B.; Goeta, A.E.; Araujo-Moreira, F.M.; Lisboa-Filho, P.N.; Pardo, H.; Andersen, K.H. *Materia* 2003, 8, 294–301.
83. Mombro, A.W.; Goeta, A.E.; Pardo, H.; Lisboa-Filho, P.N.; Suescun, L.; Mariezcurrena, R.A.; Ventura, O.N.; Behak, R.; Andersen, K.H.; Araujo-Moreira, F.M. *J. Solid State Chem.* 2002, 166, 251–258.
84. Pissas, M.; Psykharis, V.; Mitros, C.; Kallias, G.; Niarchos, D.; Simopoulos, A.; Kostikas, A. *J. Magn. Magn. Mater.* 1992, 104–107, 571–572.
85. Shannon, R.D.; Prewitt, C.T. *Acta Crystallogr. B* 1969, 25, 946–960.
86. Klyndyuk, A.I., Chizhova, E.A. *Inorg. Mater.* 2006, 42, 436–442.
87. Chizhova, E.A.; Klyndyuk, A.I.; Bashkirov, L.A.; Petrov, G.S.; Yanushkevich, K.I. *Rus. J. Appl. Chem.* 2005, 78, 702–706.
88. Atanassova, Y.K.; Popov, V.N.; Bogachev, G.G.; Iliev, M.N.; Mitros, C.; Psykharis, V.; Pissas, M. *Phys. Rev. B.* 1993, 47, 15201–15207
89. Klyndyuk, A.I., Chizhova, E.A. *Glass Phys. Chem.* 2008, 34, 313–318.
90. Trukhanov, S.V.; Trukhanov, A.V.; Szymczak, H.; Szymczak, R.; Baran, M. *J. Phys. Chem. Solids* 2006, 67, 675–681.
91. Klyndyuk, A.I. *Phys. Solid State* 2008, 50, 609–614.
92. Klyndyuk, A.I. *Rus. J. Inorg. Chem.* 2007, 52, 1343–1349.
93. Barbey, L.; Nguyen, N.; Caignaert, V.; Studer, F.; Raveau, B. *J. Solid State Chem.* 1994, 112, 148–156.
94. Troyanchuk, I.O.; Kasper, N.V.; Khalyavin, D.D.; Szymczak, H.; Szymczak, R.; Baran, M. *Phys. Rev. B.* 1998–I, 58, 2418–2421.
95. Frontera, C.; Garcia-Muñoz, J.L.; Llobet, A.; Aranda, M.A.G.; Rodriguez-Carvajal, J.; Respaud, M.; Broto, J.M.; Raquet, B.; Rakoto, H.; Goiran, M. *J. Alloys Comp.* 2001, 323–324, 468–471.
96. Zhou, H.D.; Goodenough, J.B. *J. Solid State Chem* 2004, 177, 3339–3345.
97. Mombro, A.W.; Prassides, K.; Christides, C.; Erwin, R.; Pissas, M.; Mitros, C.; Niarchos, D. *J. Phys.: Condens. Matter.* 1998, 10, 1247–1258.
98. Chizhova, Ye.A.; Klyndyuk, A.I. *Vestsi NAN Belarusi. Ser. khim. navuk.* 2009, 2, 10–14.
99. Nakamura, J.; Linden, J.; Karppinen, M.; Yamauchi, H. *Appl. Phys. Lett.* 2000, 77, 1683–1685.
100. Linden, J.; Karen, P.; Nakamura, J.; Karppinen, M.; Yamauchi, H. *Phys. Rev. B.* 2006, 73, 064415 (7 pp).
101. Taskin, A.A.; Lavrov, A.N.; Ando, Yo. *Phys. Rev. B.* 2006, 73, 121101R (4 pp).
102. Castañer, R.; Prieto, C.; Ramirez, R.; Mompean, F.; Martinez, J.L.; Ruiz-Aragon, M.J.; Amador, U. *J. Alloys Comp.* 2001, 323–324, 102–106.
103. Bourgoin, J.C.; Frossati, G.; Ravex, A.; Thoulouze, D.; Vandorpe, M.; Vaksmann, B. *Phys. Stat. Solidi (A)* 1979, 92, 585–590.
104. Klyndyuk, A.I., Chizhova, E.A. *Phys. Solid State* 2008, 50, 603–608.
105. Itoh, M.; Hashimoto, J.; Yamaguchi, S.; Tokura, Y. *Physica B* 2000, 281&282, 510–511.
106. Mott, N.F.; Davis, E.A. *Electron Processes in Non-Crystalline Materials*; Clarendon Press: Oxford, UK, 1979, 59–60.
107. Othaki, M. In: *Oxide Thermoelectrics*; Kunihiro, K.; Terasaki, I.; Murayama, N.; Eds.; Research Signpost: Trivandrum, IN, 2002; 159–180.
108. Park, K.; Jang, K.U.; Kwon, H.-C.; Kim, J.-G.; Cho, W.-S. *J. Alloys and Comp.* 2006, 419, 213–219.
109. Iwasaki, K.; Yamane, H.; Takahashi, J.; Kubota, S.; Nagasaki, T.; Arita, Y.; Nishi, Y.; Matsui, T.; Shimada, M. *J. Phys. Chem. Solids* 2005, 66, 303–307.
110. Mikami, M.; Funahashi, R. *J. Solid State Chem.* 2005, 178, 1670–1674.
111. Lu, D.; Chen, G.; Pei, J.; Yang, X.; Xian, H. *J. Rare Earth* 2008, 26, 168–172.
112. Robert, R.; Bocher, L.; Trottmann, M.; Reller, A.; Weidenkaff, A. *J. Solid State Chem.* 2006, 179, 3893–3899.

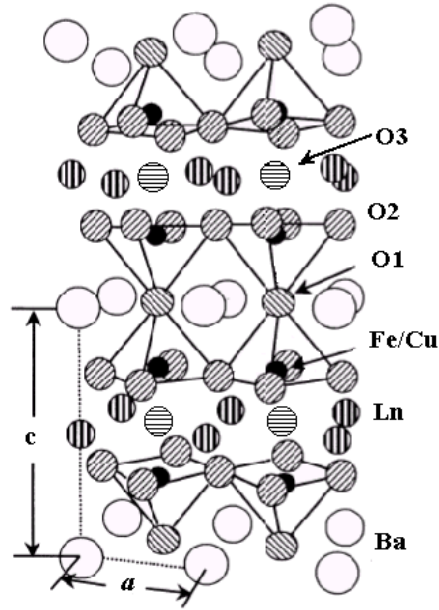


Figure 1. Crystal structure of the  $LnBaFeCuO_{5+\delta}$  (0112) phase. The O(3) positions are partially occupied.

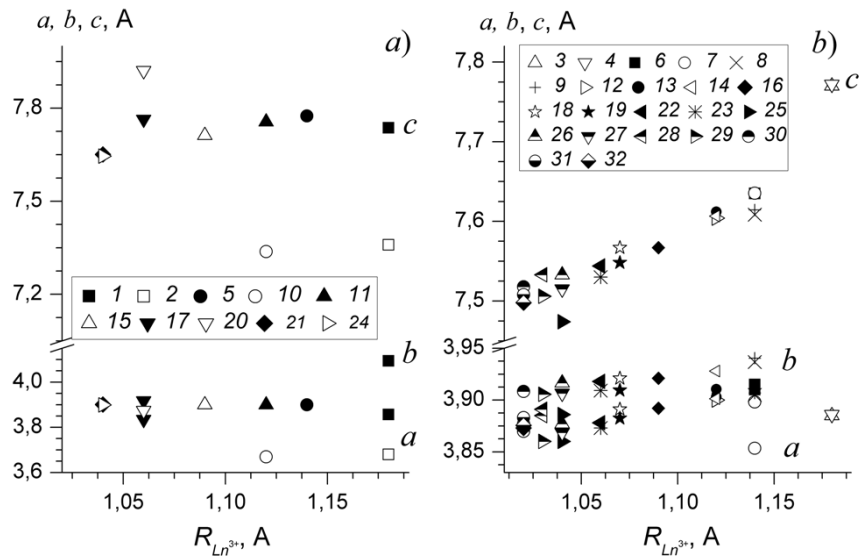


Figure 3. Dependences of the  $LnBaMn_2O_{5+\delta}$  (a) and  $LnBaCo_2O_{5+\delta}$  (b) lattice constants ( $a$ ,  $b$ ,  $c$ ) versus REE ionic radii ( $R_{Ln^{3+}}$ ) [85]:  $Ln = La$  (1) [40], (2) [41], (3) [49], (4) [28]; Pr (5) [25], (6) [28], (7) [51], (8) [53], (9) [14]; Nd (10) [41], (11) [25], (12) [49], (13) [28], (14) [57]; Sm (15) [25], (16) [27]; Eu (17) [25], (18) [28], (19) [50]; Gd (20) [42], (21) [25], (22) [28], (23) [54]; Tb (24) [25], (25) [49], (26) [28], (27) [55]; Dy (28) [28], (29) [52]; Ho (30) [56], (31) [26], (32) [52]. The data are presented in the format:  $a < b \approx a_p$ ,  $c \approx 2a_p$ .

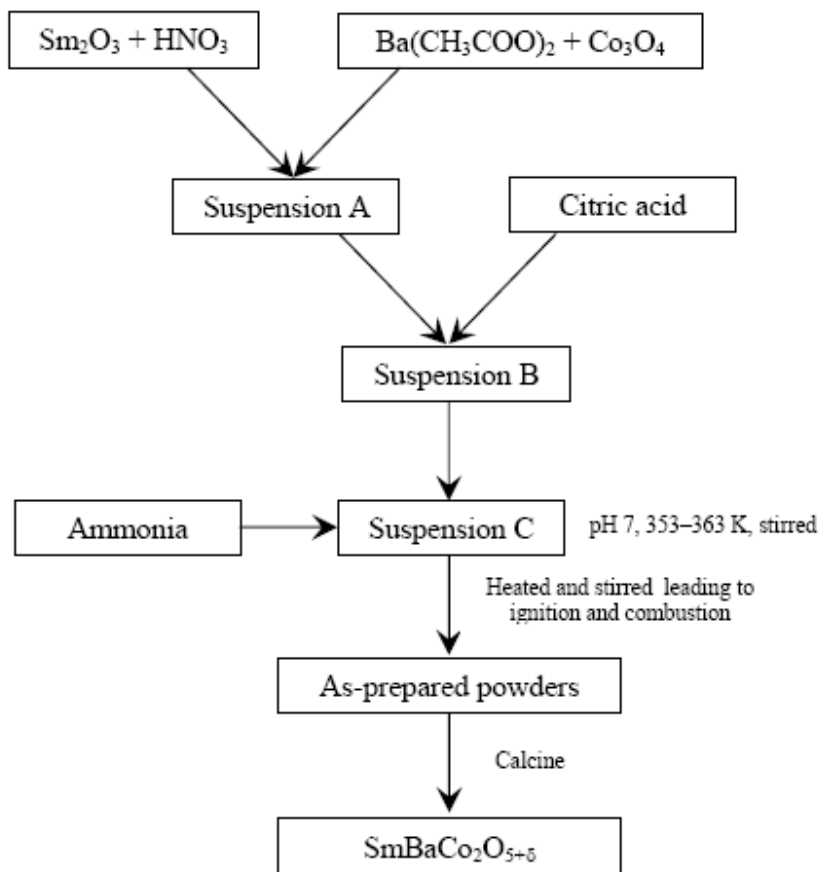


Figure 2. Procedure for the preparation of  $\text{SmBaCo}_2\text{O}_{5+\delta}$  powder [29].

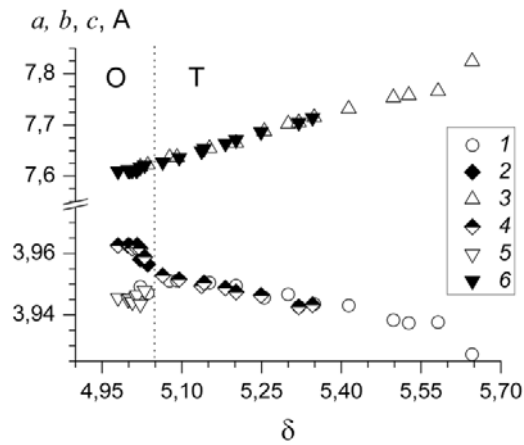


Figure 4. Dependences of the  $\text{SmBaFe}_2\text{O}_{5+\delta}$  lattice constants ( $a$ ,  $b$ ,  $c$ ) versus oxygen non-stoichiometry index ( $\delta$ ):  $a$  (1) [45], (4) [44];  $b$  (2) [45], (5) [44];  $c$  (3) [45], (6) [44]. The existence regions of orthorhombic (O) and tetragonal (T) modifications are shown.

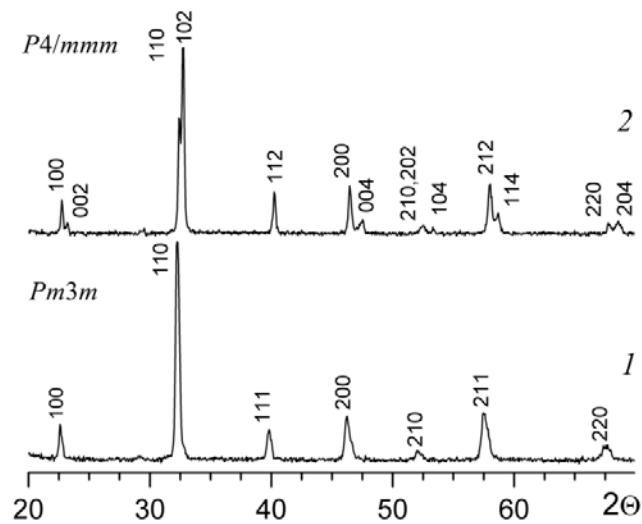


Figure 5. XRD patterns ( $\text{CuK}\alpha$ -radiation) of the  $\text{LaBaCoCuO}_{5.62}$  (1) and  $\text{NdBaCoCuO}_{5.21}$  (2) layered perovskites.

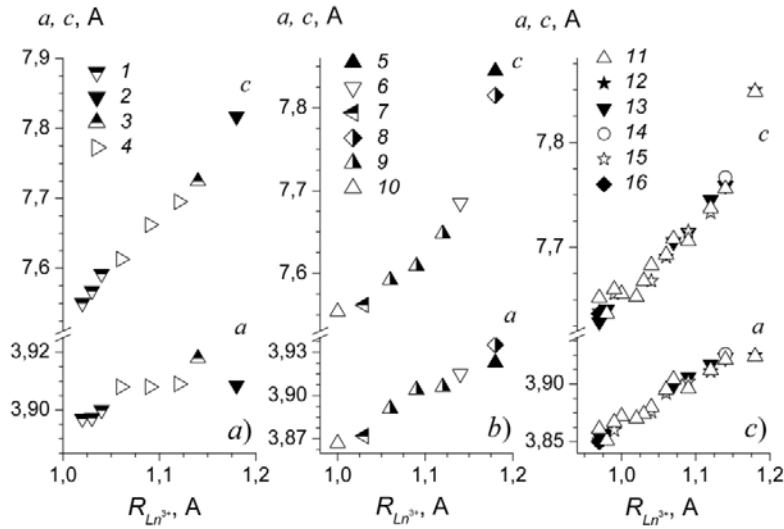


Figure 6. Dependences of the  $\text{LnBaFeCoO}_{5+\delta}$  (a),  $\text{LnBaCoCuO}_{5+\delta}$  (b) and  $\text{LnBaFeCuO}_{5+\delta}$  (c) lattice constants ( $a$ ,  $c$ ) versus REE ionic radii ( $R_{\text{Ln}^{3+}}$ ) [85]: (1) [59], (2) [63], (3) [64], (4) [21], (5) [63], (6) [64], (7) [66], (8) [67], (9) [61], (10) [69], (11) [60], (12) [79], (13) [71], (14) [81], (15) [75], (16) [84]. The data are presented in the format:  $a = b \approx a_p$ ,  $c \approx 2a_p$ .

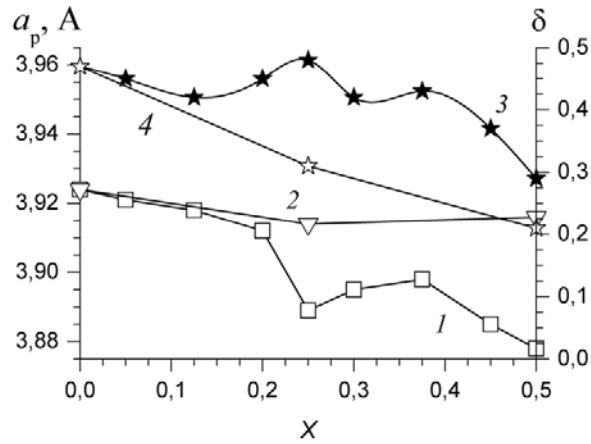


Figure 7. Dependences of  $\text{LaBa}_{1-x}\text{Me}_x\text{FeCuO}_{5+\delta}$  (Me – Sr, Mg) solid solutions lattice constant ( $a_p$ ) (1, 2) and oxygen non-stoichiometry index ( $\delta$ ) (3, 4) versus substitution degree of Ba by Sr (1, 3) or Mg (2, 4). The well-defined extrema on the  $a_p = f(x)$  and  $\delta = f(x)$  dependences for Me = Sr is caused by formation of new chemical compound  $\text{LaBa}_{3/4}\text{Sr}_{1/4}\text{FeCuO}_{5+\delta}$  [86].

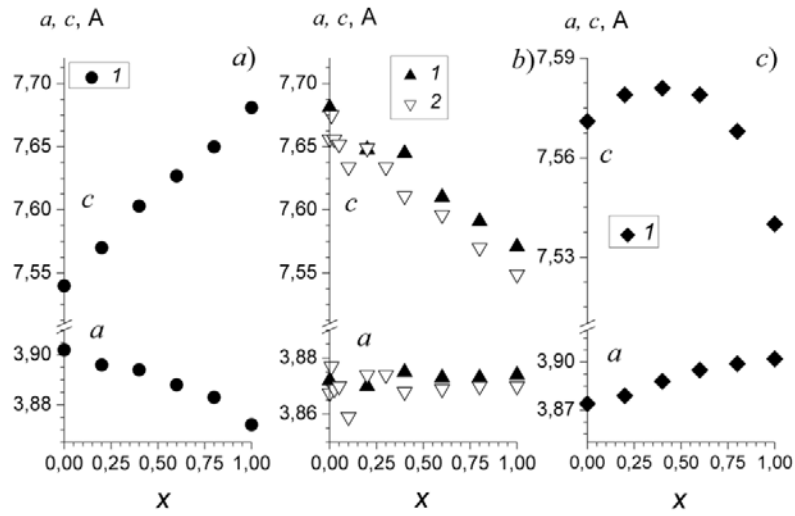


Figure 8. Dependences of the lattice constants ( $a$ ,  $c$ ) versus substitution degree ( $x$ ) for  $\text{YBaFeCo}_{1-x}\text{Cu}_x\text{O}_{5+\delta}$  (a),  $\text{YBaFe}_{1-x}\text{Co}_x\text{CuO}_{5+\delta}$  (b) and  $\text{YBaFe}_x\text{CoCu}_{1-x}\text{O}_{5+\delta}$  (c) solid solutions: (1) [65], (2) [87].

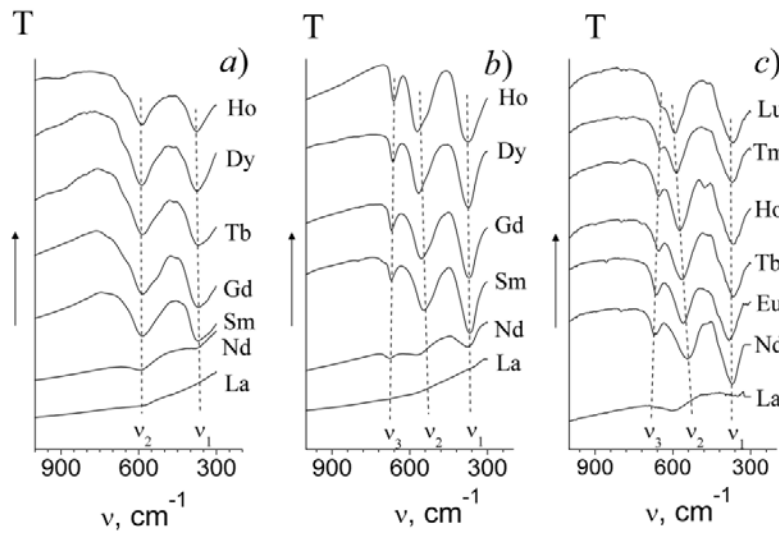


Figure 9. IR absorption spectra of the  $\text{LnBaFeCoO}_{5+\delta}$  (a),  $\text{LnBaCoCuO}_{5+\delta}$  (b) and  $\text{LnBaFeCuO}_{5+\delta}$  (c) layered perovskites [21,59–61,64,66,69].

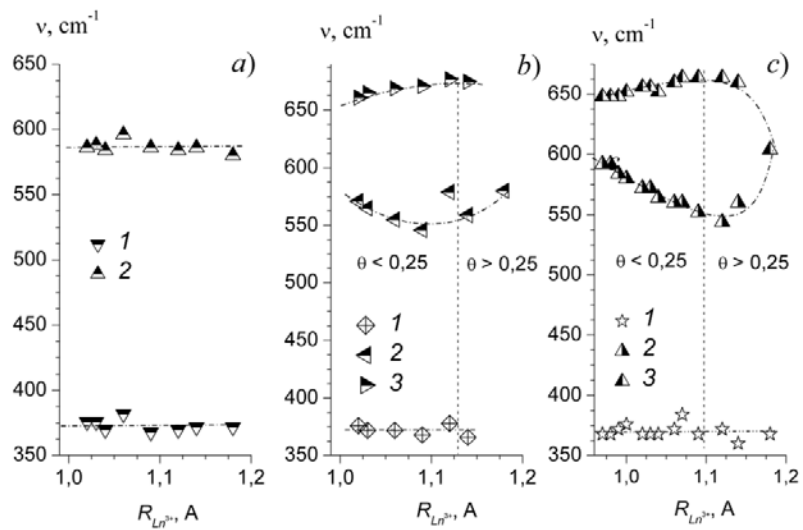


Figure 10. Dependences of the IR absorption spectra maximum of the  $LnBaFeCoO_{5+\delta}$  (a),  $LnBaCoCuO_{5+\delta}$  (b) and  $LnBaFeCuO_{5+\delta}$  (c) layered perovskites versus REE ionic radii ( $R_{Ln^{3+}}$ ) [85]:  $\nu_1$  (1),  $\nu_2$  (2)  $\nu_3$  (3) [59–61,63,64,66,69].  $\Theta$  is the occupation degree of the O(3) positions in the 0112 phases crystal structure.

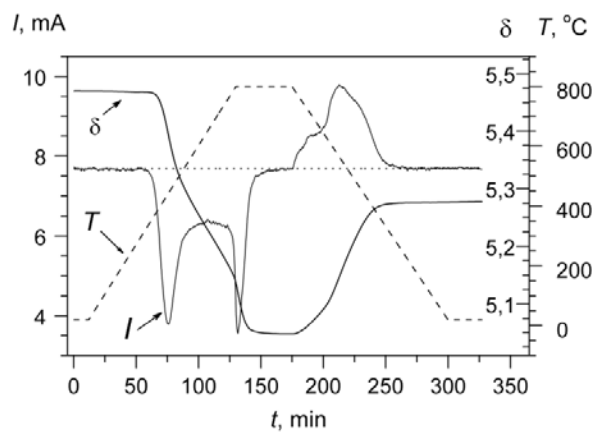


Figure 11. Change of the titration current ( $I$ ) and oxygen non-stoichiometry index ( $\delta$ ) of  $LaBaFeCuO_{5+\delta}$  powder during heating and cooling in argon ( $p_{O_2} = 1000$  Pa). The results were obtained using coulometric complex Oxylyt, SensoTech (Germany).

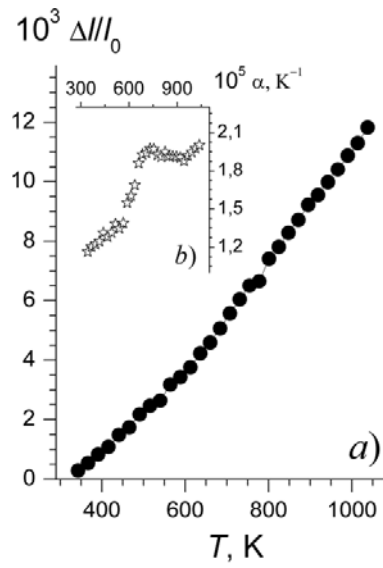


Figure 12. Temperature dependences of the relative elongation ( $\Delta l/l_0$ ) (a) and linear thermal expansion coefficient ( $\alpha$ ) (b) of  $\text{NdBaCoCuO}_{5+\delta}$  layered perovskite in air.

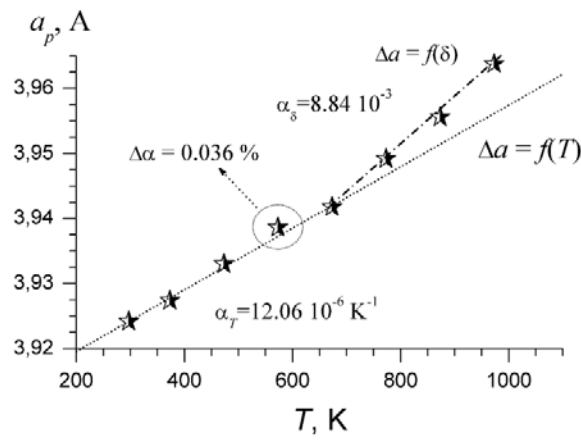


Figure 13. Temperature dependence of the  $\text{LaBaFeCuO}_{5+\delta}$  unit cell parameter ( $a_p$ ). The separation of the thermal ( $\alpha_T$ ) and chemical ( $\alpha_\delta$ ) expansion coefficient as well as the jump  $\Delta a_p$  as a result of the oxygen disorder also is shown (acc. to [92]).

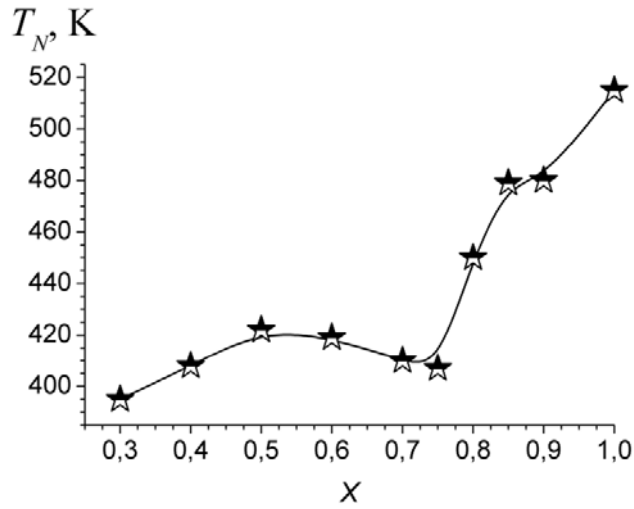


Figure 14. Dependence of the Neel temperature ( $T_N$ ) versus Cu content ( $x$ ) for  $\text{YBaCo}_{2-x}\text{Cu}_x\text{O}_5$  solid solutions [93].

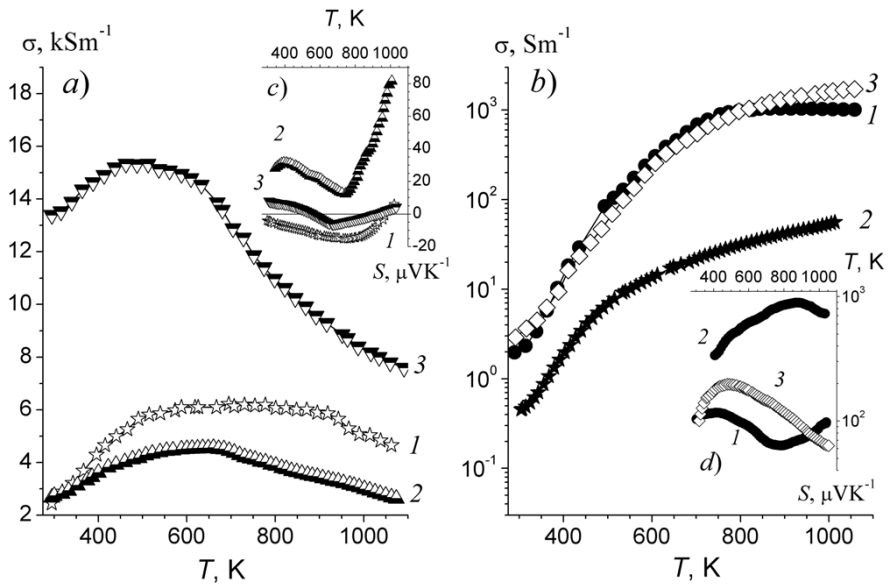


Figure 15. Temperature dependences of electrical conductivity ( $\sigma$ ) (a, c) and thermo-e.m.f. ( $S$ ) (b, d) for  $\text{LaBaMe}'\text{Me}''\text{O}_{5+\delta}$  (a, b) and  $\text{YBaMe}'\text{Me}''\text{O}_{5+\delta}$  (c, d) phases:  $\text{Me}'\text{Me}'' = \text{FeCo}$  (1) [59,63],  $\text{FeCu}$  (2) [104],  $\text{CoCu}$  (3) [63,66].

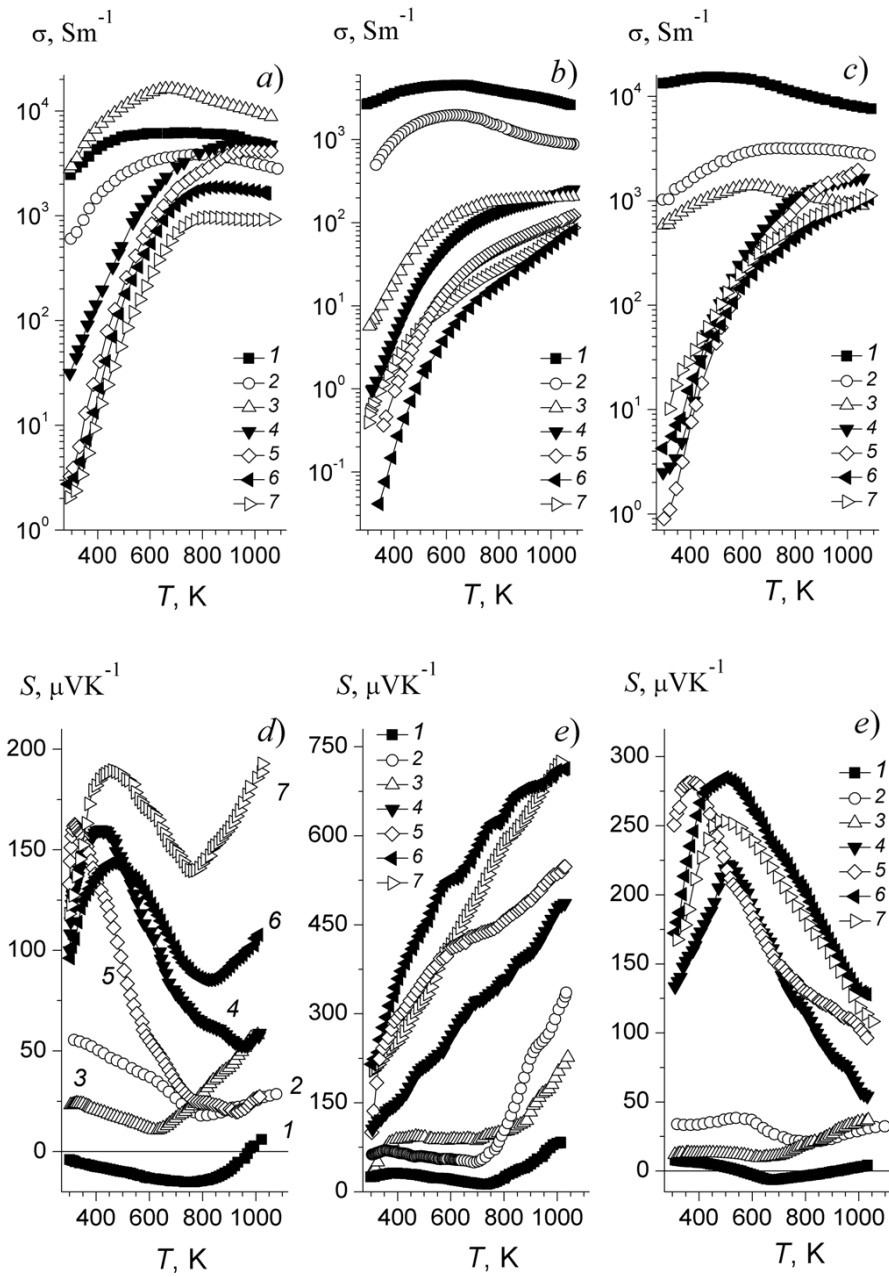


Figure 16. Temperature dependences of electrical conductivity ( $\sigma$ )(*a, b, c*) and thermo-e.m.f. (*S*) (*d, e, f*) for  $LnBaFeCoFeO_{5+\delta}$  (*a, d*),  $LnBaFeCuFeO_{5+\delta}$  (*b, e*)  $LnBaCoCuFeO_{5+\delta}$  (*c, f*) layered perovskites:  $Ln = La$  (1) [22,63], Pr (2) [22,64], Nd (3) [21,22,61], Sm (4) [21,22,61], Gd (5) [21,22,61], Dy (6) [22,59,66], Ho (7) [22,59,69].

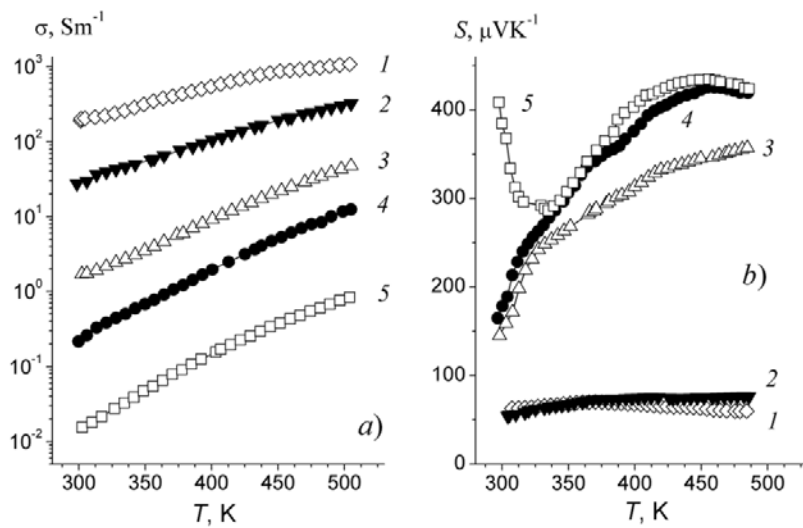


Figure 17. Temperature dependences of electrical conductivity ( $\sigma$ ) (a) and thermo-e.m.f. ( $S$ ) (b) for  $\text{PrBaFeCuO}_{5+\delta}$ :  $\delta = 0,28$  (1),  $0,19$  (2),  $0,11$  (3),  $0,02$  (4),  $0,00$  (5) (acc. to [91]).

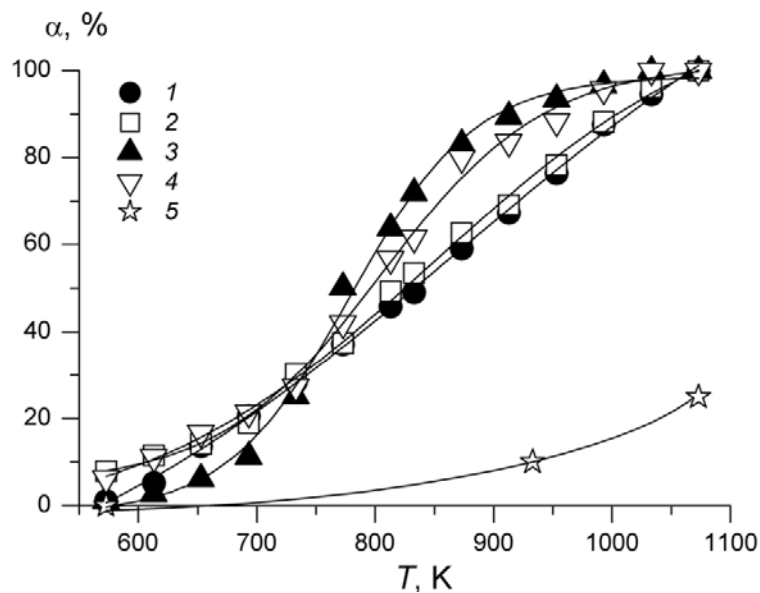


Figure 18. Temperature dependences of conversion degree of propane–butane mixture by its oxidation of atmospheric oxygen (gas volume rate  $3,6 \cdot 10^4 \text{ h}^{-1}$ , hydrocarbons content – 0.1 vol. %) with (1–4) and without (5) solid catalysts:  $\text{YBaCuFeO}_5$  (1),  $\text{YBaFe}_{0,9}\text{Mn}_{0,01}\text{O}_5$  (2),  $\text{YBaFe}_{0,9}\text{Co}_{0,1}\text{O}_5$  (3),  $\text{YBaFe}_{0,9}\text{Ni}_{0,1}\text{O}_5$  (4) (acc. to [15]).

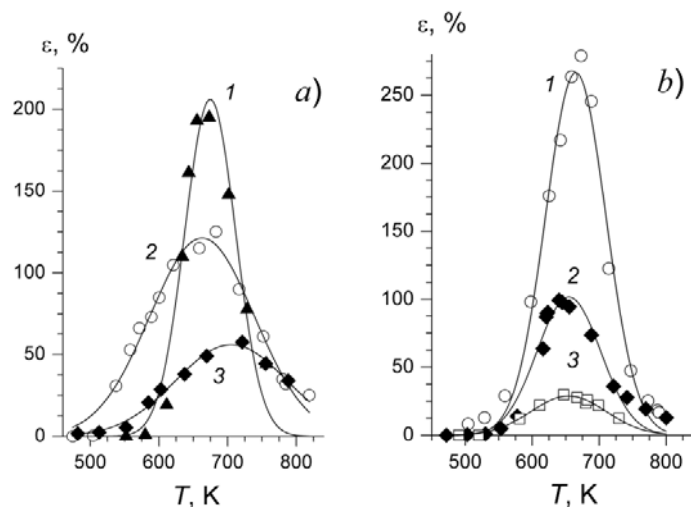


Figure 19. Temperature dependences of the response of the layered perovskite thick films  $\text{LaBaCuFe}_{0.9}\text{Mn}_{0.1}\text{O}_{5+\delta}$  (a) and  $\text{LaBaCuFe}_{0.9}\text{Ni}_{0.1}\text{O}_{5+\delta}$  (b) to the presence in air vapors of  $\text{CH}_3\text{COCH}_2\text{COCH}_3$  (150 ppm) (1), 1,4- $\text{C}_4\text{H}_8\text{O}_2$  (750 ppm) (2) and  $\text{C}_4\text{H}_9\text{OH}$  (75 ppm) (3) (according to [6,16]).

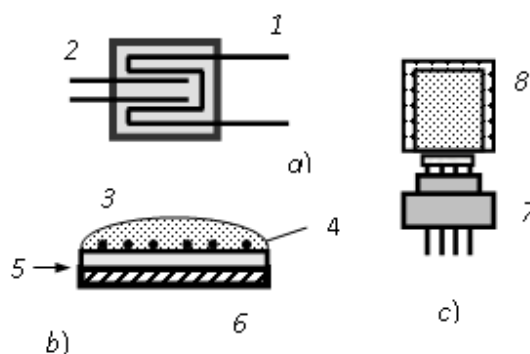


Figure 20. Schema of the working element of chemical gas sensor: a – view from the top, b – view from the side (in a cut), c – sensor in assemblage: 1 – Pt heater, 2 – Pt electrodes, 3 – active layer, 4 –  $\text{SiO}_2$ , 5 – Si substrate, 6 – case, 7 – protective cap.

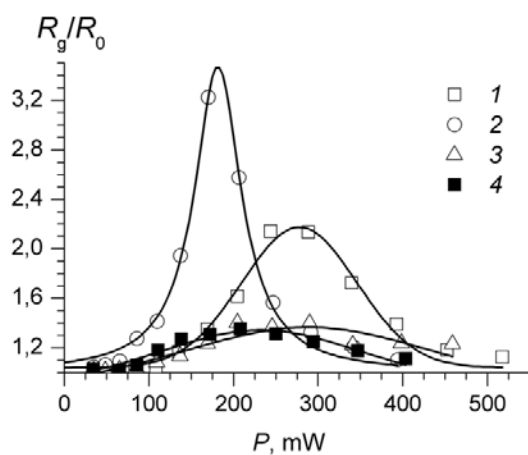


Figure 21. Power dependences of response of gas sensor with working element based on  $\text{YBaCuFe}_{0.8}\text{Ni}_{0.2}\text{O}_{5+\delta}$  to the presence in air vapors of  $\text{C}_2\text{H}_5\text{OH}$  (0.4 vol. %) (1),  $\text{CH}_3\text{COCH}_2\text{COCH}_3$  (740 ppm) (2),  $\text{NH}_3$  (7.9 vol. %) (3),  $1,4\text{-C}_4\text{H}_8\text{O}_2$  (0.4 vol. %) (4) (acc. to [16]).

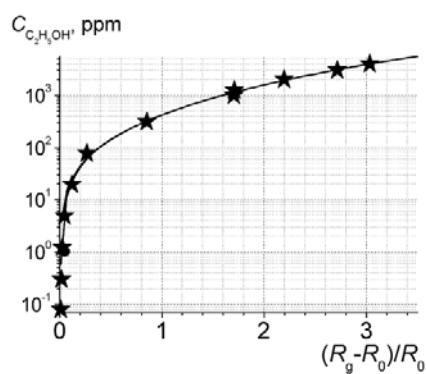


Figure 22. Dependence of content of ethanol vapor in air ( $\text{C}_2\text{H}_5\text{OH}$ ) versus response of gas sensor based on  $\text{YBaCuFe}_{0.8}\text{Ni}_{0.2}\text{O}_{5+\delta}$  ( $(R_g - R_0)/R_0$ ). Heater power is 300 mW (acc. to [16]).

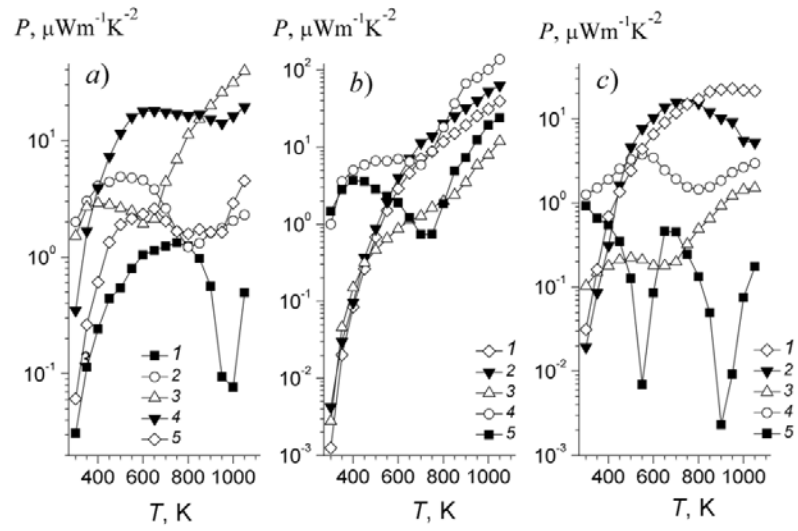


Figure 23. Temperature dependences of power factor ( $P$ ) for  $LnBaFeCoFeO_{5+\delta}$  (a),  $LnBaFeCuFeO_{5+\delta}$  (b)  $LnBaCoCuFeO_{5+\delta}$  (c) layered perovskites:  $Ln = La$  (1), Pr (2), Nd (3), Sm (4), Gd (5) (calculated from data [21,22,61,63,64]).